

Heavy Neutrino as Dark Matter in a Neutrinophilic $U(1)$ Model

Waleed Abdallah,^{1,*} Anjan Kumar Barik,^{2,†} Santosh Kumar Rai,^{2,‡} and Tousik Samui^{3,§}

¹*Department of Mathematics, Faculty of Science, Cairo University, Giza 12613, Egypt.*

²*Regional Centre for Accelerator-based Particle Physics, Harish-Chandra Research Institute,
A CI of Homi Bhabha National Institute,
Chhatnag Road, Jhansi, Prayagraj 211019, India.*

³*Department of Physical Sciences, Indian Institute of Science Education and Research Kolkata,
Mohanpur 741 246, India.*

Abstract

We study the prospect of heavy singlet neutrinos as a dark matter (DM) candidate within a neutrinophilic $U(1)$ model, where the Standard Model (SM) is extended with a $U(1)$ gauge symmetry, and neutrino mass and oscillation parameters are explained through an inverse see-saw mechanism. The lightest of the heavy neutrinos plays the role of the DM while the newly introduced scalars and the extra gauge boson Z' act as mediators between the dark sector and the SM sector. We show the range of model parameters where this DM candidate can be accommodated in the Weakly Interacting Massive Particle (WIMP) or Feebly Interacting Massive Particle (FIMP) scenario. The observed DM relic density is achieved via the new gauge boson and singlet scalar portals in the WIMP scenario whereas within the FIMP scenario, these two particles assume a distinct yet pivotal role in generating the observed relic density of dark matter.

arXiv:2405.15333v1 [hep-ph] 24 May 2024

* awaleed@sci.cu.edu.eg

† anjanbarik@hri.res.in

‡ skrai@hri.res.in

§ tousik.pdf@iiserkol.ac.in

I. INTRODUCTION

Astrophysical observations from Coma cluster [1], galaxy rotation curves [2, 3], gravitational lensing [4] and bullet cluster [5] provide strong evidence that there is a large amount of invisible matter in our universe. This matter is believed to interact very weakly with the visible sector particles described successfully by the Standard Model (SM) and is called the dark matter (DM). Although very little information is available for the DM to us, it reveals some broad features; that it has gravitational interactions and it should be non-relativistic or "cold" so that it can form structures in the universe. Additionally, WMAP [6] data indicates that DM contributes roughly 27% of the universe's energy budget, compared to only 5% for visible matter. The energy density of the DM is expressed in terms of its relic density (RD), which is measured to be 0.1198 ± 0.0012 [7].

Despite its key importance in modern cosmology, the nature of the DM remains elusive to us. While the DM is known to have gravitational interactions, other interactions, *viz.* strong and electroweak interactions of the DM sector are expected to be very feeble to accommodate its non-observation in the direct detection experiments [8–10]. Two popular hypothesized scenarios containing DM are (a) Weakly Interacting Massive Particle (WIMP) [11–13], and (b) Feebly Interacting Massive Particle (FIMP) [14]. The WIMP scenarios hypothesize a freeze-out mechanism, wherein the DM that was abundant in the early phase of the universe froze out from the thermal bath due to the expansion of the universe and remained dark to the visible sector except for its gravitational interaction. On the other hand, in the feebly interacting scenario, the DM is considered to be absent in the early universe and produced later from the SM particles. The interaction strength of the DM candidate with the visible sector particles should be feeble enough so as not to over-shoot the currently observed DM relic density. A crucial difference between these two scenarios is that the WIMPs are thought to be in the thermal bath before they freeze out while the FIMPs were never in thermal equilibrium. There are many attempts to accommodate DM within BSM frameworks (see for example [15–22]) primarily via the WIMP scenario. On the other hand, attempts to explain the DM in the FIMP scenario are relatively new (see for example [14, 23–35]). In this work, we study a neutrinophilic model [36], which can accommodate WIMP and FIMP in different parameter regions. This model considers an extra $U(1)$ gauge symmetry, the simplest gauge extension of the SM. Models with an extra $U(1)$ symmetry can have their roots in grand unified theories [37–40], where one starts with groups of higher ranks that leave an additional $U(1)$ after the spontaneous symmetry breaking. On the other hand, in the more simplistic bottom-up approach, one adds the $U(1)$ to the SM gauge group. The typical feature of such $U(1)$ models

is the appearance of an extra massive gauge boson Z' and additional scalars responsible for the spontaneous breaking of the additional symmetry.

The model in consideration is primarily motivated to provide a solution to the neutrino mass and mixing puzzle. The light neutrinos get their mass via the inverse see-saw mechanism in the presence of heavy sterile neutrinos that provide the Majorana term to facilitate the tiny masses. The lightest heavy sterile neutrino can act as a cold DM (CDM) in this scenario. The production of such DM in the early universe and their interaction with the SM particles then depends on its interactions via the Z' and the new scalars in the model. The signature of this model at the Large Hadron Collider (LHC) was studied in Ref. [36, 41] where the role of gauge-kinetic mixing was considered. In the latter work, we also showed the viability of the heavy neutrinos as DM candidates in the model. In this work, we discuss in more detail the prospects of the heavy sterile neutrinos as DM and their role as a WIMP or FIMP.

The rest of the article is organized as follows. In section II, we describe the model briefly with a focus on the DM aspect of the model. Section III contains the discussion of the WIMP scenario and the detection of such a model in the current and upcoming experiments. In section IV, we explore the possibility of the FIMP scenario in a certain parameter space of the model. We then summarize and conclude in section V.

II. THE MODEL

We consider a neutrinophilic model [36, 41], which is an extension of the SM gauge symmetry with a new $U(1)_X$ gauge symmetry. The SM particles do not transform under the new gauge symmetry. The new particles in this model are a second Higgs doublet, a scalar singlet, and three vector-like fermions. The charge assignment of the particles is shown in Table I.

The gauge invariant Lagrangian containing the new fields and the SM like Higgs doublet (denoted by H_1) is given as

$$\begin{aligned} \mathcal{L} \supset & (D_\mu H_1)^\dagger D_\mu H_1 + (D_\mu H_2)^\dagger D_\mu H_2 + (D_\mu S)^\dagger D_\mu S - \mu_1 H_1^\dagger H_1 - \mu_2 H_2^\dagger H_2 - \mu_s S^\dagger S \\ & + \{\mu_{12} H_1^\dagger H_2 + \text{h.c.}\} - \lambda_1 (H_1^\dagger H_1)^2 - \lambda_2 (H_2^\dagger H_2)^2 - \lambda_s (S^\dagger S)^2 - \lambda'_{12} \left| H_1^\dagger H_2 \right|^2 - \lambda_{12} H_1^\dagger H_1 H_2^\dagger H_2 \\ & - \lambda_{1s} H_1^\dagger H_1 S^\dagger S - \lambda_{2s} H_2^\dagger H_2 S^\dagger S - \{Y_\nu \bar{l}_L H_2 N_R + Y_R S \bar{N}_R N_R^C + Y_L S \bar{N}_L N_L^C + \text{h.c.}\}. \end{aligned} \quad (1)$$

Note that the μ_{12} term which *a priori* breaks the $U(1)_X$ symmetry in the Lagrangian is dynamically generated through an additional scalar S_2 . S_2 is singlet under the SM gauge symmetry and has $U(1)_X$ charge opposite to the H_2 so that a gauge invariant term $\mu_3 H_1^\dagger H_2 S_2$ can be added in the

Fields	$SU(3)_C$	$SU(2)_L$	$U(1)_Y$	$U(1)_X$	Spin
N_L^i	1	1	0	q_x	1/2
N_R^i	1	1	0	q_x	1/2
H_1	1	2	-1/2	0	0
H_2	1	2	-1/2	$-q_x$	0
S	1	1	0	$2q_x$	0
S_2	1	1	0	q_x	0

TABLE I. New fields and their charge assignments under the SM gauge group and $U(1)_X$.

Lagrangian and therefore the softly broken term $\mu_{12} = \mu_3 \langle S_2 \rangle$ can be obtained when S_2 acquires vacuum expectation value. As the new scalar would simply introduce extra terms in the Lagrangian, it is assumed to be heavy to keep the model minimal and has been excluded from the Lagrangian shown in Eq. (1). The masses for the scalars are obtained after the spontaneous symmetry breaking of the scalar potential term of Eq. (1). Considering the vacuum expectation values (vev) for the scalars H_1 , H_2 , and S to be v_1 , v_2 , and v_s , respectively, the mass matrix for the CP-even scalar becomes

$$M_H^2 = \begin{pmatrix} 2\lambda_1 v_1^2 + \mu_{12} \frac{v_2}{v_1} & (\lambda_{12} + \lambda'_{12}) v_1 v_2 - \mu_{12} & \lambda_{1s} v_1 v_s \\ (\lambda_{12} + \lambda'_{12}) v_1 v_2 - \mu_{12} & 2\lambda_2 v_2^2 + \mu_{12} \frac{v_1}{v_2} & \lambda_{2s} v_2 v_s \\ \lambda_{1s} v_1 v_s & \lambda_{2s} v_2 v_s & 2\lambda_s v_s^2 \end{pmatrix}, \quad (2)$$

After diagonalization via 3×3 unitary mixing matrix Z^h , the physical eigenstates are represented by h_1 , h_2 , and h_s to represent the states dominated by the neutral CP-even components of H_1 , H_2 and S , respectively. In our scenario, we identify h_1 to be the observed 125-GeV scalar [42, 43] at the LHC. The other two are kept heavier than 125 GeV. The masses for pseudo-scalar A and the charged scalar H^\pm can be expressed as

$$M_A^2 = \frac{\mu_{12}}{v_1 v_2} v^2 = \frac{2\mu_{12}}{\sin 2\beta}, \quad (3)$$

$$M_{H^\pm}^2 = \left(\frac{\mu_{12}}{v_1 v_2} - \frac{\lambda'_{12}}{2} \right) v^2 = m_A^2 - \frac{\lambda'_{12}}{2} v^2, \quad (4)$$

where $v = \sqrt{v_1^2 + v_2^2} \simeq 246$ GeV. In the general two Higgs Doublet model type setups, it is conventional to parametrize the vevs v_1 and v_2 in terms of v and $\tan \beta \equiv v_2/v_1$ ¹.

¹ In the most common two Higgs Doublet Model convention prefers to align the SM Higgs doublet with H_2 . Hence, a higher $\tan \beta$ value is preferable in those setups. Our convention is opposite to the most common convention; therefore, a low $\tan \beta$ region is preferable.

A gauge-kinetic mixing (GKM) term of the form $\frac{1}{2}\tilde{g}B^{\mu\nu}C_{\mu\nu}$ between $U(1)_Y$ gauge boson B_μ and the new gauge boson can be introduced in the Lagrangian as it is gauge invariant [44, 45]. The kinetic term for the gauge boson with the inclusion of the GKM term can be written as

$$\mathcal{L} \supset -\frac{1}{4}G^{a,\mu\nu}G_{\mu\nu}^a - \frac{1}{4}W^{b,\mu\nu}W_{\mu\nu}^b - \frac{1}{4}B^{\mu\nu}B_{\mu\nu} - \frac{1}{4}C^{\mu\nu}C_{\mu\nu} + \frac{1}{2}\tilde{g}B^{\mu\nu}C_{\mu\nu}, \quad (5)$$

The spontaneous breaking of gauge symmetry leads to massive gauge bosons in the particle spectrum. The $SU(2) \times U(1)$ gauge symmetry is spontaneously broken to $U(1)_{\text{em}}$ when H_1 and H_2 acquired vev, whereas the additional $U(1)_X$ gauge symmetry is spontaneously broken when S and H_2 obtain vev. The new $U(1)_X$ gauge boson mixes with the SM neutral gauge bosons. The masses of the physical gauge bosons Z and Z' can be expressed as

$$M_{Z,Z'}^2 = \frac{1}{8} \left[g_z^2 v^2 + g_x'^2 v^2 + 4g_x g_x' v_2^2 + 4g_x^2 (v_2^2 + 4v_s^2) \right] \mp \frac{1}{8} \sqrt{\left(g_x'^2 v^2 + 4g_x g_x' v_2^2 + 4g_x^2 (v_2^2 + 4v_s^2) - g_z^2 v^2 \right)^2 + 4g_z^2 \left(g_x' v^2 + 2g_x v_2^2 \right)^2}, \quad (6)$$

where $g_z = \sqrt{g_1^2 + g_2^2}$, and $g_x' = \frac{g_1 \tilde{g}}{\sqrt{1 - \tilde{g}^2}}$. The coupling constants for $U(1)_Y$, $SU(2)$ and $U(1)_X$ gauge groups are g_1 , g_2 and $g_x \sqrt{1 - \tilde{g}}$, respectively². The mixing angle between Z and Z' is given by

$$\tan 2\theta' = \frac{2g_z (g_x' v^2 + 2g_x v_2^2)}{g_x'^2 v^2 + 4g_x g_x' v_2^2 + 4g_x^2 (v_2^2 + 4v_s^2) - g_z^2 v^2} \simeq \frac{(2g_x \tan^2 \beta + g_x') M_Z^2}{M_{Z'}^2 - M_Z^2}, \quad (7)$$

The electroweak precision observables, as well as precise measurement of Z boson decay width puts an upper limit of 10^{-3} on the mixing angle θ' [46].

Recall the terms for the neutrinos in the Lagrangian density in Eq. (1):

$$\mathcal{L} \supset -Y_\nu \bar{l}_L H_2 N_R - Y_R S \bar{N}_R N_R^C - Y_L S \bar{N}_L N_L^C - M_N \bar{N}_L N_R + \text{h.c.} \quad (8)$$

where N_R and N_L are 3-generations of sterile neutrinos and Y_ν, Y_L , and Y_R are Yukawa couplings of the form 3×3 matrices. After symmetry breaking, the mass term for the neutrino sector becomes

$$\mathcal{L}_\nu^{\text{mass}} = -\frac{v_2}{\sqrt{2}} Y_\nu \bar{\nu}_L N_R - \frac{v_s}{\sqrt{2}} Y_R \bar{N}_R^C N_R - M_N \bar{N}_L N_R - \frac{v_s}{\sqrt{2}} Y_L \bar{N}_L^C N_L + \text{h.c.} \quad (9)$$

The neutrino mass matrix in $(\nu_L \ N_R^C \ N_L)^T$ basis, therefore, becomes

$$\mathcal{M}_\nu = \begin{pmatrix} 0 & m_D^T & 0 \\ m_D & m_R & M_N \\ 0 & M_N^T & m_L \end{pmatrix}, \quad (10)$$

² The redefinition of the original coupling g_x was needed to receive simplified expressions; for more details, see Ref. [36].

with $m_D = v_2 Y_\nu / \sqrt{2}$, $m_R = \sqrt{2} v_s Y_R$ and $m_L = \sqrt{2} v_s Y_L$. For $m_L, m_R \ll m_D, M_N$, the expressions for masses of the neutrinos become

$$m_{\nu_\ell} \simeq \frac{m_D^2 m_L}{M_N^2 + m_D^2}, \quad (11)$$

$$m_{\nu_{H,H'}} \simeq \frac{1}{2} \left(\frac{M_N^2 m_L}{M_N^2 + m_D^2} + m_R \right) \mp \sqrt{M_N^2 + m_D^2}, \quad (12)$$

where we represent ν_ℓ to be light neutrinos and $\nu_{H,H'}$ to be the heavier ones. For simplicity we have chosen $Y_R = 0$. The $\mathcal{O}(0.1)$ eV neutrino mass can be achieved with the following choices

$$Y_\nu \sim \mathcal{O}(0.1), \quad M_N \sim 1 \text{ TeV}, \quad \text{and} \quad m_L \sim \mathcal{O}(10^{-6}) \text{ GeV}.$$

We find that the model can accommodate a DM candidate from a pair of heavy neutrinos $\nu_{4(5)}$. As there is no symmetry which prevents them from decay we have the decaying DM scenario in this model. These heavy neutrinos can decay to $l^\pm W^\mp$, νZ due to their mixing with the SM neutrinos. As these decay channels of DM can yield high energy neutrino flux therefore the strongest bound on the life time of the DM comes from the IceCube collaboration which is $\mathcal{O}(10^{28})$ s [47–50]. Therefore, the lightest of them (ν_4) becomes stable or long-lived if the corresponding Yukawa Y_ν couplings are very small. For simplicity we consider Y_ν and M_N to be diagonal. The total decay width of the lightest heavy neutrino when $M_4 > M_Z$ is approximately given by [51]

$$\Gamma_{\nu_4} \approx |V_{14}|^2 \frac{3G_F M_4^3}{8\pi\sqrt{2}} \quad (13)$$

with $|V_{14}| = \mathcal{O}(\frac{m_D}{M_N})$ [36]. The IceCube bound on Γ_{ν_4} then translates into an upper bound for $Y_\nu < 4.7 \times 10^{-26} \times \frac{1}{\sin\beta} \sqrt{\frac{\text{GeV}}{M_4}}$. A viable choice that leads to a stable ν_4 can be $Y_{\nu_{11}} \simeq 10^{-27}$ and $Y_{\nu_{1j}} = 0$ has been considered through out the subsequent analysis. The ν_5 also has a similar set of interactions as it is connected to ν_4 via $M_{N_{11}}$. A degenerate ν_5 will therefore be also stable like ν_4 . In this work, we concentrate on one component DM scenario. Therefore, we choose $Y_{L_{11}}$ in such a way that a mass splitting of a few MeV to a few GeV between ν_4 and ν_5 is generated, that allows ν_5 to decay to ν_4 and a light SM fermion anti-fermion pair via off-shell Z or Z' . Since there is a mixing between the SM Higgs boson and the other two BSM scalars, the above can also be mediated by these heavy scalars. As the interaction between DM and visible sector is mediated by the the singlet scalar and the Z' , the DM production and annihilation are dominated by the s -channel diagrams with propagator Z' and h_i 's.

III. WIMP SCENARIO

Weakly interacting massive particles have been proposed to address the DM puzzle, and in this scenario the WIMPs are usually massive compared to the bath particles. Their scattering cross-sections are in the range of weak interaction cross-sections suggesting that the WIMP was in thermal equilibrium with SM particles in the early universe. As the universe cools down because of the Hubble expansion, the equilibrium number density of a particle species changes with time. When the temperature of the universe becomes comparable to WIMP mass, the rate of the creation of DM from the annihilation of the bath particles is suppressed. This happens because the fraction of the number density of equilibrium particles that possess such high momentum to produce DM pair is Boltzmann suppressed. The co-moving number density of DM continues to change until the rate of all the DM number changing processes become much smaller compared to the Hubble expansion rate.

The evolution of the number density n_k of a particle species k due to the expansion of the universe and its interaction with other particles is described by Boltzmann equation [23]

$$\frac{dn_k}{dt} + 3Hn_k = R_k(t), \quad (14)$$

where H is the Hubble expansion rate and $R_k(t)$ is the collision term containing decay and (co)annihilation processes. When the dark sector contains additional particles with masses close to the mass of the DM, the Boltzmann equation for the number density of these additional particles need to be taken into consideration, as the co-annihilation processes can change the total dark sector density. We can obtain the present DM number density by solving the coupled Boltzmann equations for the dark sector particles. The coupled form of the equations comes via the collision term, which incorporates decay and (co)annihilation processes [52]. For a particular particle species, one can then calculate, via the evolution equations, its present relic density (RD). This is defined as the ratio of the present energy density to the critical energy density [53],

$$\Omega_X = \frac{\rho_0}{\rho_c} = \frac{m_X n_X^0}{\rho_c} = \frac{m_X Y_X^0 s_0}{\rho_c}, \quad \rho_c \equiv \frac{3H_0^2}{8\pi G},$$

where ρ_c is the critical energy density, $s_0 = 2.8912 \times 10^9 \text{ m}^{-3}$ gives the entropy density, and $H_0 = 100 h \text{ km s}^{-1} \text{ Mpc}^{-1}$ with $h = 0.678(9)$, is the Hubble constant in present time. The present yield Y_X^0 for particle species X is $Y_X^0 \equiv \frac{n_X^0}{s_0}$.

In this work, we consider the lightest (ν_4) of the heavy sterile neutrinos to be the DM candidate. While the next lightest state (ν_5) mass is kept close to the ν_4 mass, the remaining sterile neutrinos

are kept much heavier than these two. So we ignore the heavier states as only ν_4 and ν_5 will play the most important role in our analysis for DM. The ν_4 and ν_5 interact with the SM particles only through the Z' and the singlet dominated scalar h_s and they can (co)annihilate to the visible sector through the s -channel via Z' and h_s . There is significant enhancement in the (co)annihilation cross-section when the heavy neutrino mass becomes half of the s -channel mediator's mass. This gives a funnel-like shape in the DM relic density distribution near $M_{Z'}/2$ or $M_{h_s}/2$ when plotted as a function of DM mass. Therefore, we have two situations which we refer to as Z' -funnel and scalar-funnel scenarios depending on the mediator responsible for the funnel shape. In the following analysis, we study the annihilation channels of both the aforementioned scenarios.

We used `SARAH` [54] to implement the Lagrangian and `SPheno` [55] for the generation of a spectrum of parameters and masses. We have then used `micrOMEGAs` [56] to calculate the DM abundance.

A. Z' -funnel

In this section, we study the DM freeze-out when they annihilate to the visible sector, primarily through the s -channel exchange of Z' . The expression for the coupling of Z' with SM fermions and scalars are given in Appendix A. Note that the SM fermion coupling to the Z' depends on both the GKM parameter g'_x and the Z - Z' mixing angle θ' . The precise measurement of Z boson decay width at LEP put a strong constraint on the value of θ' to be below $< 10^{-3}$ [46]. This bound suppresses the coupling strength of Z' with SM fermions containing θ' . However the GKM parameter g'_x can still have large values and dictate the couplings of Z' to the SM fermions, thus enabling the DM to primarily annihilate to the SM fermions via the Z' propagator. The Z' coupling to SM gauge bosons also depend on θ' and its coupling to W^+W^- and $h_i Z$ are given in the appendix. In the vanishing GKM scenario, the possibility of DM annihilating to the SM fermions via Z' is less. However, the presence of non-zero coupling of Z' to the scalars of the model allows the DM to annihilate into these scalars. We explore these two scenarios *viz.* (a) nonzero GKM and (b) vanishing GKM in detail.

1. Non-zero GKM

In this scenario we keep a non-vanishing value for the gauge kinetic mixing. In our WIMP scenario the masses for both the DM and the Z' are chosen to be in the range of a few hundred

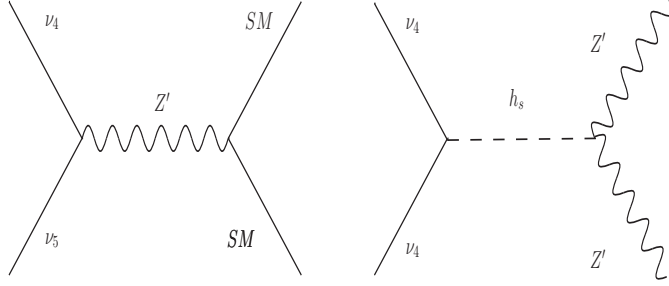


FIG. 1. DM (co)annihilation process through Z' and h_s resonances with SM particles and Z' 's in the final state respectively.

GeV. We have further checked that ν_5 is not stable but is very long-lived. The relevant annihilation channels for our study are

$$\nu_4\nu_5 \rightarrow W^+W^-, \quad \nu_4\nu_5 \rightarrow hZ, \quad \text{and} \quad \nu_4\nu_5 \rightarrow f\bar{f}, \quad (15)$$

and they contribute via non-zero Z - Z' mixing and GKM. The Feynman diagrams for the above annihilation processes are shown in Fig. 2. To demonstrate the Z' -funnel, we first show, in

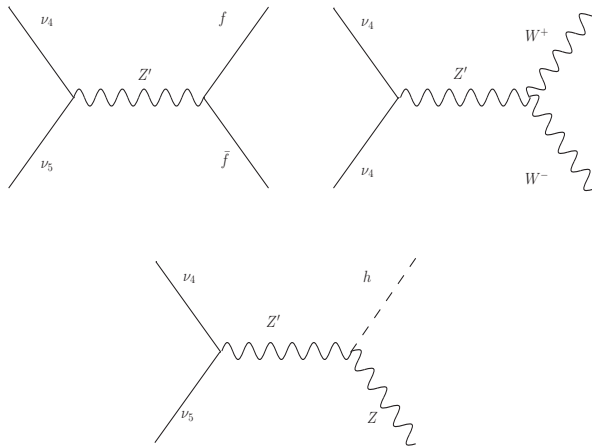


FIG. 2. Feynman diagrams for ν_4, ν_5 co-annihilation to SM particles via Z' .

Fig. 3(a), the variation of the DM relic density Ωh^2 as a function of the mass of the DM. We choose three different values of $M_{Z'} = \{250, 500, 750\}$ GeV while the GKM parameter $g'_x = \{4, 8, 12\} \times 10^{-3}$ to show the relic density dependence on the propagator mass and coupling strengths. The mass gap between ν_4 and ν_5 is of $\mathcal{O}(\text{MeV})$, with $v_S = 1$ TeV, $Y_{L11} = 10^{-5}$. The $\nu_4\nu_4 Z'$, $\nu_4\nu_5 Z'$ and $\nu_5\nu_5 Z'$ couplings strength depend on the mass splitting between ν_4 and ν_5 as shown in Fig.4. The dominant channel is therefore $\nu_4\nu_5 \rightarrow f\bar{f}$ as they co-annihilate. A clear dip is visible in the DM relic at $M_{\text{DM}} \simeq M_{Z'}/2$. This is due to the s -channel resonance enhancement of the annihilation

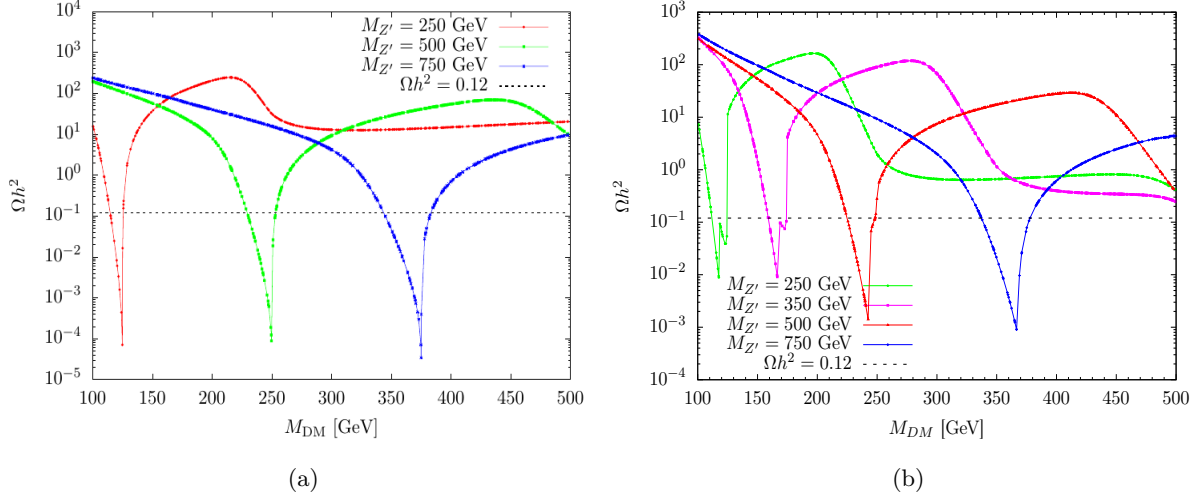


FIG. 3. The Dark Matter Relic Density (DMRD), denoted as Ωh^2 , is plotted against the Dark Matter (DM) mass for three different values of $M_{Z'}$. The mass gap between ν_4 and ν_5 is approximately of the order of a few MeV on the left plot and around 10 GeV on the right plot.

cross-section. An interesting feature is that the funnel becomes wider as we go to a higher mass of Z' because of the increase in decay width of the Z' boson. The DM relic density curve is not symmetric about the lowest point of Z' funnel. In the region $M_{DM} < M_{Z'}/2$, as DM mass approaches the funnel region the Ωh^2 decreases since the DM annihilation can produce on-shell Z' as it possesses some kinetic energy to reach up to the resonance. As soon as we go to the region $M_{DM} > M_{Z'}/2$, two DM particles cannot produce a single Z' on-shell as it is kinematically forbidden. As a result, it is sharply increasing on the right of the resonance. We notice a fall in

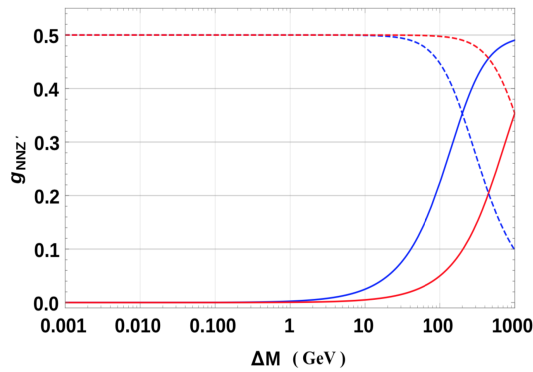


FIG. 4. The variation of $\nu_4\nu_4 Z'$ (solid line) and $\nu_4\nu_5 Z'$ (dashed line) couplings as a function of $\Delta M = M_{\nu_5} - M_{\nu_4}$, with $g_x = 1$. The results are presented for two values of $M_{N_{11}}$: 100 GeV (blue) and 500 GeV (red).

DM relic density near $M_{\text{DM}} \simeq M_{Z'}$. This is because of the t-channel DM annihilation processes $\nu_4\nu_4 \rightarrow Z'Z'$ and $\nu_5\nu_5 \rightarrow Z'Z'$ become kinematically allowed.

We now consider the scenario where we have a $\mathcal{O}(10 \text{ GeV})$ mass difference between ν_4 and ν_5 . To calculate the relic density we scan over the following ranges of the relevant parameters:

$$M_{N_{11}} \in [100, 500] \text{ GeV}, \quad g_x \in [0.2, 1.0], \quad g'_x \in [-0.05, 0.05],$$

$$\tan \beta = 10^{-2}, \quad \text{and} \quad v_s = 502.5 \text{ GeV}. \quad (16)$$

Note that the smaller value for the vev v_s allows a larger coupling strength g_x , compared to the previous scenario where the vev was 1 TeV. This has a direct effect on the total decay width of the mediating gauge boson Z' . Fig. 3(b) shows the DM relic density as a function of the DM mass for four different values of $M_{Z'}$: 250, 350, 500, and 750 GeV with $g'_x = \{4, 4, 8, 12\} \times 10^{-3}$ respectively. For the mass gap of $\mathcal{O}(10 \text{ GeV})$ between ν_5 and ν_4 , with $Y_{L_{11}} = 2 \times 10^{-2}$, the distribution of the relic density is very similar to the in Fig. 3(a). As expected, the DM relic density has a dip near $M_{\text{DM}} \simeq M_{Z'} - M_{\nu_5}$ due to the co-annihilation of ν_4 and ν_5 via Z' channel. Additionally, a second dip appears near $M_{\text{DM}} \simeq M_{Z'}/2$. This second dip is much more prominent for $M_{Z'} = 250 \text{ GeV}$ and $M_{Z'} = 350 \text{ GeV}$. Note that with a larger mass splitting between ν_4 and ν_5 , there is a non-zero and sizeable $\nu_4\nu_4Z'$ interaction. However, as the DM mass increases, the coupling strength diminishes for a given mass difference between ν_4 and ν_5 (see Fig. 4). As we go to higher values of the DM mass, the ν_4 and ν_4 annihilation process is not efficient enough to obtain the correct DM relic density. Therefore the depth of the second funnel decreases with an increase in DM mass. For $M_{Z'} = 500 \text{ GeV}$ and $M_{Z'} = 750 \text{ GeV}$, the annihilation effect is less prominent.

We have performed a scan over the parameter regions mentioned in Eq. (16). We show the DM relic density in the Ωh^2 - $(M_{Z'} - 2M_{\text{DM}})$ plane in Fig. 5(a) for $|m_{\nu_5} - m_{\nu_4}|$ of $\mathcal{O}(10 \text{ GeV})$. The plot shows that the DM relic density can be satisfied only when $M_{\text{DM}} \simeq M_{Z'}/2$, which we call Z' -funnel region. Furthermore, in general, the DMRD is less in the funnel region compared to the regions left and right to it. This is expected since the annihilation of DM occurs through on-shell Z' boson with a larger rate and, therefore, the DMRD becomes less after the freeze-out. Clearly, most of the points are outside the funnel region have overabundant DMRD value. However, many points in the funnel region satisfy the observed DMRD.

The same data points have been plotted in Ωh^2 - M_{DM} plane in Fig. 5(b) for $|m_{\nu_5} - m_{\nu_4}| \sim 10 \text{ GeV}$, and g'_x on the colour bar. The red points, which are close to $g'_x = 0$, are overabundant as, in that region, the interaction of SM fields with Z' , which only depend on θ' , is very small. Hence, the DM annihilation via this channel is not efficient enough to give the correct DMRD. We also notice

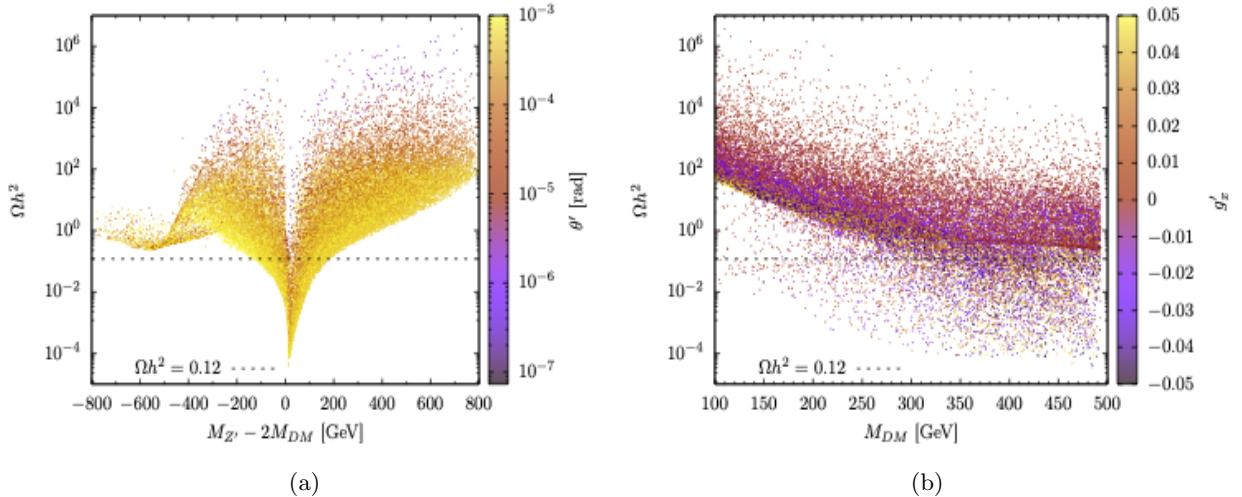


FIG. 5. (a) Dip in the DMRD occur at $M_{Z'} \simeq 2M_{DM}$. (b) The DMRD Ωh^2 as a function of DM mass and GKM g'_x .

that, there are a large number of points satisfying DMRD in the heavier DM region compared to the lighter DM region. A comparison between the Figs. 5(a) and 5(b) reveals that heavier Z' prefers the correct- and under-relic points. This is because, in the light $M_{Z'}$ region, the value of g'_x needs to be small in order to keep the Z - Z' mixing angle θ' below 10^{-3} . As a result, DM annihilation is suppressed, leading to higher RD. On the other hand, a heavy Z' can accommodate higher values of GKM while staying within the θ' upper limit. Hence, the DMRD is less due to its high annihilation with high GKM.

2. Vanishing GKM

We now move to study the DM phenomenology when $g'_x \simeq 0$. For this scenario, we have varied the following parameters in the given range:

$$M_{N_{11}} \in [100, 500] \text{ GeV}, \quad g_x \in [0.1, 1.0], \quad \text{and} \quad \tan \beta \in [0.01, 3], \quad (17)$$

while fixing $Y_{L_{11}} = 2 \times 10^{-2}$ and other scalar sector parameters. As μ_{12} has been kept fixed, the masses of physical scalars from H_2 can be varied by the parameter $\tan \beta$. The scalar quartic couplings λ_{12} and λ'_{12} are kept small (5×10^{-3}), so that the physical scalars from H_2 (h_2, A, H^\pm) will have nearly degenerate mass. Since GKM is vanishingly small, the Z' will interact with the SM fermions only through θ' (see Appendix A for Feynman rules). Therefore, this mixing angle depends on the VEV of H_2 , i.e. on $\tan \beta$ and $M_{Z'}$, as can be seen from Eq. (7). One can then check that, for a fixed value of $M_{Z'}$, the value of θ' increases as $\tan \beta$ increases. Hence, Z' coupling

with the SM fermions become stronger as we increase $\tan\beta$. Therefore, to satisfy the observed DMRD, one needs an increased $\tan\beta$, which enhances DM annihilation via Z' to the SM modes. However, such a large value of $\tan\beta$ is ruled out for lighter Z' by the requirement of $\theta' < 10^{-3}$. In addition large $\tan\beta$ can also alter the SM Higgs signal strength. In the region scanned for $\tan\beta \in [0.01, 3]$, we find that the allowed range of $\tan\beta \in [0.01, 0.14]$ that satisfies the constraints from various scalar searches at collider experiments and Higgs signal strength. We have checked these experimental constraints using `HiggsBounds` [57, 58] and `HiggsSignals` [59].

The small value of θ' would prevent the DM from annihilating to the SM fields, which could have led to an overabundant scenario. However, coupling of the Z' to the scalars comes to our rescue. Therefore, in the vanishing GKM scenario, the most dominant DM (co)annihilation processes, through Z' propagator are

$$\nu_4\nu_5 \rightarrow H^+H^-/h_2A/h_2Z/H^\pm W^\mp/h_1A. \quad (18)$$

Some representative Feynman diagrams of these processes are shown in Fig. 6(a). To show the funnel region, we have plotted the parameter points in the Ωh^2 -($M_{Z'} - 2M_{\text{DM}}$) plane in Fig. 6(b). All these points satisfy the scalar sector constraints. The first two processes ($\nu_4\nu_5 \rightarrow H^+H^-/h_2A$) are dominant when $M_{Z'} > 2M_{H^\pm}$ and $M_{Z'} > M_{h_2} + M_A$. This is illustrated in Fig. 6(c), where the DMRD is lower in the lighter M_{H^\pm} region. Since μ_{12} is fixed, therefore, a smaller M_{H^\pm} corresponds to larger $\tan\beta$, which is evident from the figure and the equation 3. On the other hand, the vertex containing two gauge bosons and one scalar involves two gauge couplings and a vev, making the third and fourth processes, ($\nu_4\nu_5 \rightarrow h_2Z/H^\pm W^\mp$) subdominant due to the small vev of H_2 doublet. Therefore, in this region, the DM annihilation rate through these processes is higher for a smaller mass of charged Higgs. The last process, i.e. $\nu_4\nu_5 \rightarrow h_1A$, depends on the mixing angle between the neutral CP-even components of H_1, H_2 . Thus, for larger $\tan\beta$, this process has significant contribution in achieving the correct DMRD.

In the $M_{Z'} < 2M_{H^\pm}$ region, we rely on the last three processes to achieve the correct DMRD, if they are kinematically allowed. We need a larger $\tan\beta$ so that coupling strength involving two gauge bosons and a second doublet scalar get enhanced due to a larger H_2 vev. From Fig. 6(d), we find that some points with $M_{Z'} < 2M_{H^\pm}$ in the lighter region of M_{H^\pm} satisfy the relic density. In high M_{H^\pm} region (> 500 GeV), DM annihilation through these processes is ineffective due to small $\tan\beta$. Given the scan range of $M_{Z'} \in [100, 1000]$ GeV, in the region $M_{H^\pm} > 500$ GeV, Z' can not decay to H^+H^-/h_2A , leading to an overabundant scenario.

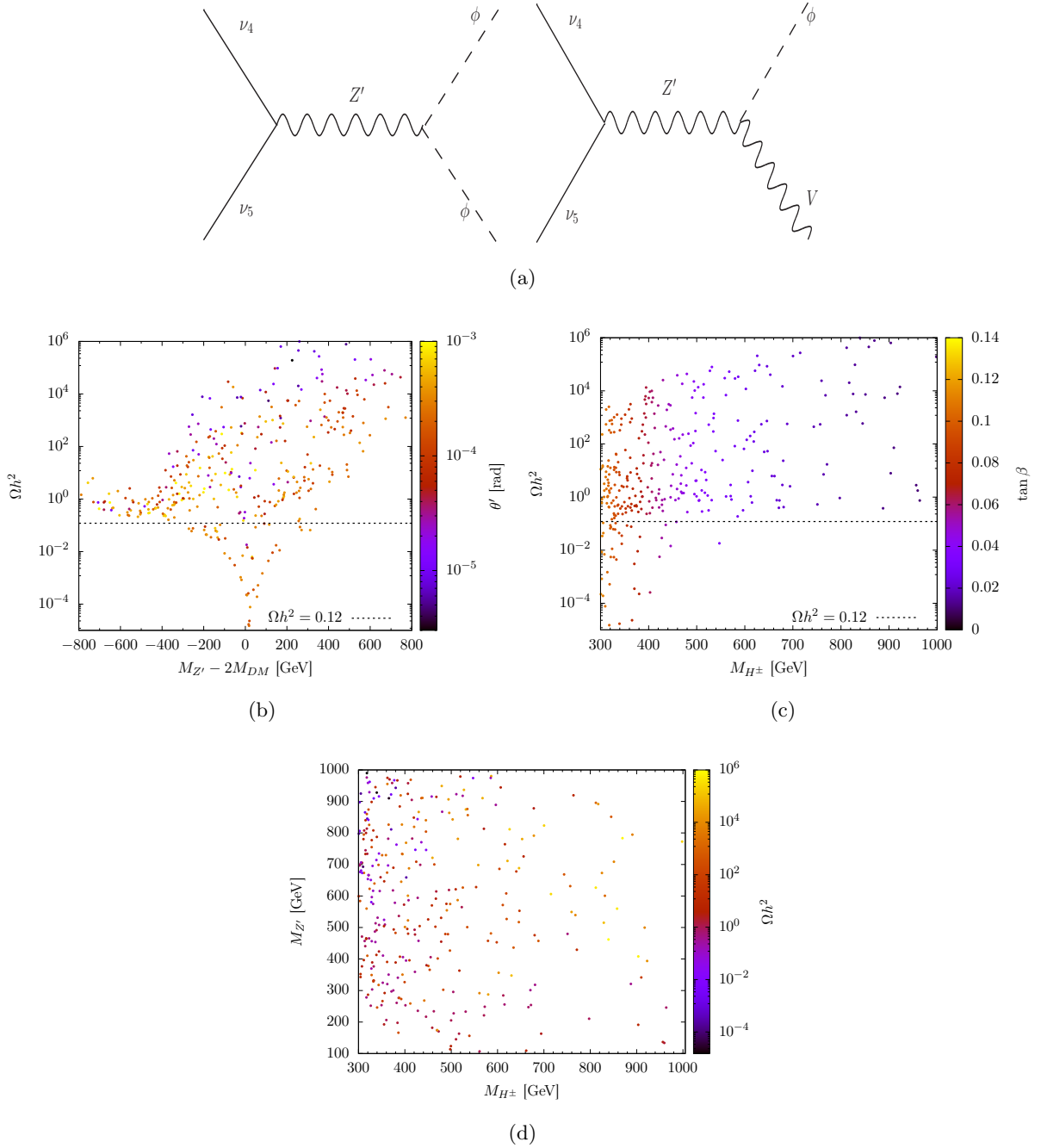


FIG. 6. (a) Feynman diagrams for DM annihilation via Z' resonance for vanishing GKM, where $\phi = h_1, h_2, A, H^\pm$ and $V = Z, W^\pm$. (b) Dip in the DMRD Ωh^2 due to resonant production of Z' . (c) Higher values of $\tan \beta$ give lighter h_2, H^\pm, A , hence DM can annihilate to them via Z' resonance. (d) Scanned points in $M_{H^\pm} - M_{Z'}$ plane with DMRD in colour bar.

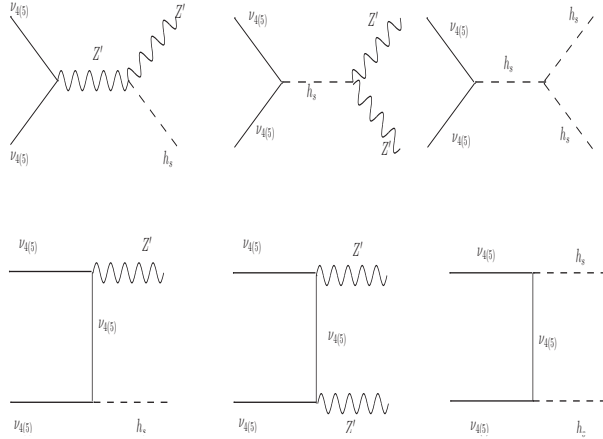


FIG. 7. The dominant annihilation channels: $\nu_4\nu_5 \rightarrow h_s Z'$ (t -channel via ν_4 and ν_5), $\nu_4\nu_4 \rightarrow Z'Z'$, $\nu_5\nu_5 \rightarrow Z'Z'$. Note that it is possible for DM annihilation through t -channels: $\nu_4\nu_5 \rightarrow h_s h_s$, $\nu_5\nu_5 \rightarrow h_s h_s$ and $\nu_4\nu_4 \rightarrow h_s h_s$.

B. Scalar funnel

In the scenarios where the Z' has weaker interaction with the SM particles or the annihilation processes discussed earlier are not kinematically feasible, the DM annihilation via Z' is not efficient enough to provide the observed DMRD. In such cases, we rely on the scalar sector parameters to obtain the correct DMRD. The ν_4 and ν_5 primarily interact with the singlet scalar (neglecting the coupling with h_2 , as it is of $\mathcal{O}(10^{-27})$) through the Yukawa coupling Y_{L11} . Additionally, they can couple to other scalars through scalar mixing. As a result, s -channel processes are possible where ν_4 and ν_5 annihilate via h_s to the SM and other visible BSM particles. Moreover, ν_4 and ν_5 can annihilate to $h_s Z'$, $Z'Z'$, and $h_s h_s$ through t -channels when these processes are kinematically allowed.

The Feynman diagrams contributing to these processes are shown in Fig. 7. The top row of the figure illustrates all the s -channel processes, with the top middle diagram potentially responsible for scalar-funnel DM annihilation. On the other hand, the bottom row shows the diagrams with the $\nu_{4(5)}$ in the t -channel. Note that the Z' propagator in the diagram corresponding to the annihilation channel $h_s Z'$, which is shown in the top-left panel, cannot be on-shell. The same is true for the diagrams contributing to $\nu_{4(5)}\nu_{4(5)} \rightarrow h_s h_s$ annihilation channel. These channels, therefore, do not contribute to the funnel region.

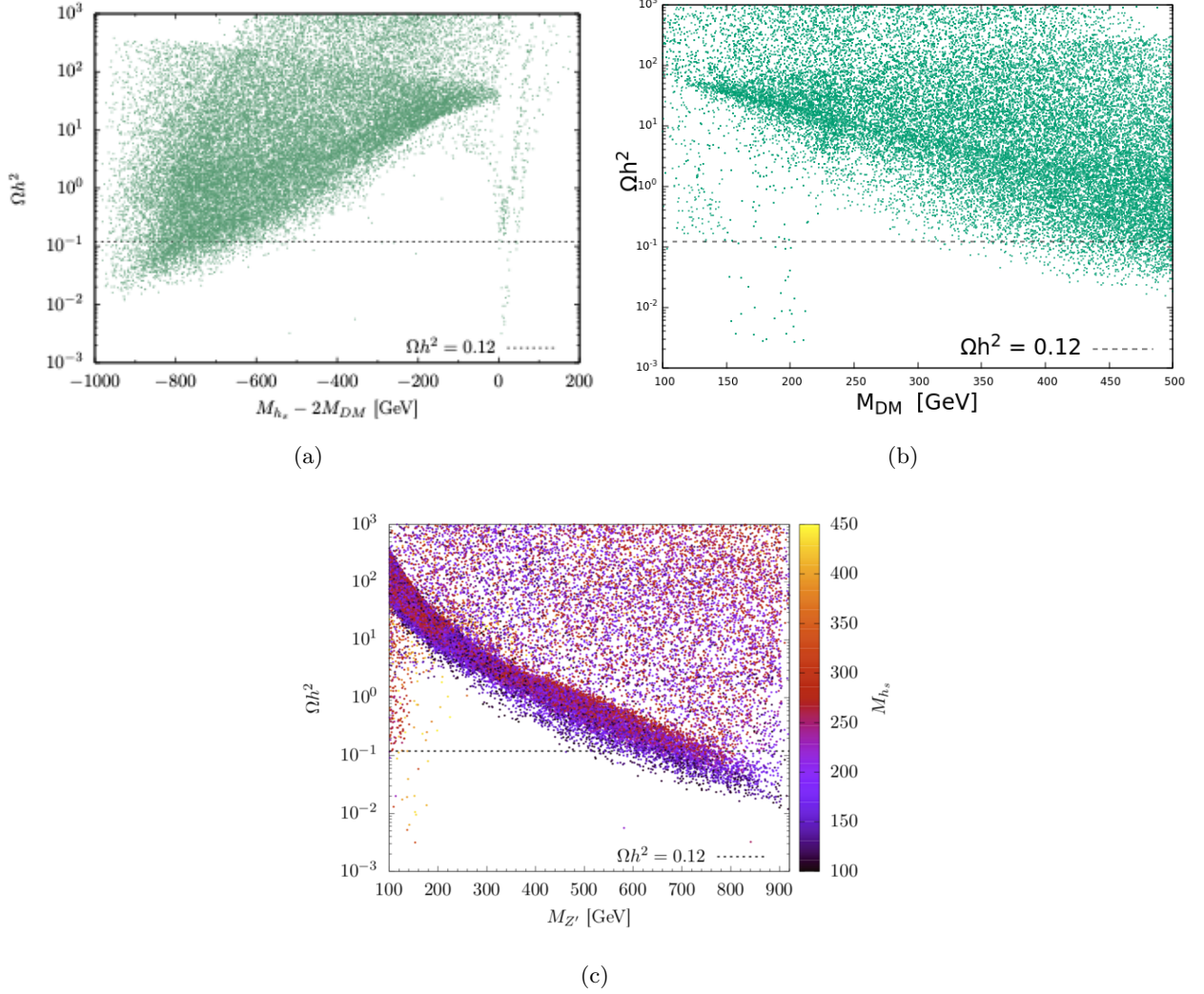


FIG. 8. (a) Dip at $M_{h_s} = 2M_{\text{DM}}$ implies, h_s is resonantly produced from DM annihilation. In region $M_{h_s} - 2M_{\text{DM}} < 400$ GeV, a DM pair dominantly annihilates to $h_s h_s$, $h_s Z'$. (b) The DMRD Ωh^2 as function of M_{DM} . (c) The DMRD Ωh^2 as a function of $M_{Z'}$ and M_{h_s} . For lighter Z' , a DM pair annihilates to $Z' Z'$ via h_s resonance while for heavy Z' , it annihilates to $h_s Z'$.

For the study of DM phenomenology, we vary the relevant parameters in the following ranges:

$$\begin{aligned}
 Y_{L11} &\in [0.005, 0.5], & M_{N11} &\in [100, 500] \text{ GeV}, \\
 M_{Z'} &\in [100, 1000] \text{ GeV}, & \text{and } M_{h_s} &\in [100, 450] \text{ GeV}.
 \end{aligned}
 \tag{19}$$

In this study, we consider $g'_x = 0$ so that the Z' coupling to the SM fields is negligible and choose $\tan\beta = 10^{-4}$ to make masses of h_2, A, H^\pm around 10 TeV when $\mu_{12} = 10^4$ GeV². This setup minimises the contribution of Z' resonance to the DMRD. The process $(\nu_{4(5)}\nu_{4(5)} \rightarrow Z' Z')$ becomes significant in the DM sector particles annihilation, when h_s is resonantly produced and

decays to two Z' bosons, thereby creating a funnel in DMRD. When the s -channel scalar resonance does not provide substantial annihilation, the other DM annihilation processes with t -channel and s -channel are effective involving $h_s Z'$, $Z' Z'$ and $h_s h_s$ in the final state. The annihilation process ($\nu_4 \nu_5 \rightarrow h_s Z'$) happens without scalar mixing as the singlet scalar was charged under $U(1)_X$. This is the most dominant annihilation channel in this parameter region of our scan, occurring via both t -channel and s -channel. The s -channel diagram, contains $Z' Z' h_s$ vertex, which is proportional to $v_s g_x^2$, making this process the most significant contributor.

Fig. 8 shows the variation of the DMRD with M_{DM} , M_{h_s} and $M_{Z'}$. In order to show the funnel region, the parameter points are plotted in Ωh^2 - $(M_{h_s} - 2M_{\text{DM}})$ plane in Fig. 8(a) where the funnel-like shape appears near $M_{h_s} - 2M_{\text{DM}} \simeq 0$ region. In this region, the dominant channel for these points is $\nu_4 \nu_4 \rightarrow h_s \rightarrow Z' Z'$ through the singlet scalar s -channel process. The points to the left of the funnel region correspond to the $\nu_4 \nu_5 \rightarrow h_s Z'$ process where the DM pair is annihilating to h_s and Z' . In Fig. 8(b), we show the same parameter points but in the Ωh^2 - M_{DM} plane. In this plot, one can see that the points corresponding to the funnel region are spread near $M_{\text{DM}} \simeq M_{Z'} \in [100, 200]$ GeV. However, the region with DM mass above 500 GeV has correct or under abundant relic density because of their annihilation to $h_s Z'$ final state. These points correspond to $M_{Z'} > 500$ GeV as can be seen from Figs. 8(c). From these two panels, we find some points are under-abundant when $M_{Z'} \in [100, 200]$ GeV with $M_{h_s} \in [250, 450]$ GeV. These points belong to the scalar funnel region. The scalar funnel region can be extended to heavier $M_{Z'}$ by increasing M_{h_s} . As the singlet scalar has a mixing of $\mathcal{O}(10^{-8})$ and smaller coupling with the other two CP even scalars, DM annihilating to SM particles or two light scalars through singlet scalar gives a negligible contribution to the the DMRD.

Fig. 8(c) shows that there are some under-abundant points with $M_{Z'} \in [500, 900]$ GeV and $M_{h_s} \in [100, 300]$ GeV. The dominant channel for these points is $\nu_4 \nu_5 \rightarrow h_s Z'$ with Z' in s -channel. For $\frac{M_{h_s}}{2} < M_{Z'} < 500$ GeV, g_x is not large enough for considerable DM annihilation. Therefore, overabundance of the DMRD occurs since the annihilation cross-section is proportional to g_x^4 .

C. DM detection

In the previous sections, we have discussed how to achieve the observed DMRD in the right ballpark via different annihilation channels. Now, we move to the observational aspects of the DM candidate in our model and the constraints coming from the DM direct and indirect detection experiments.

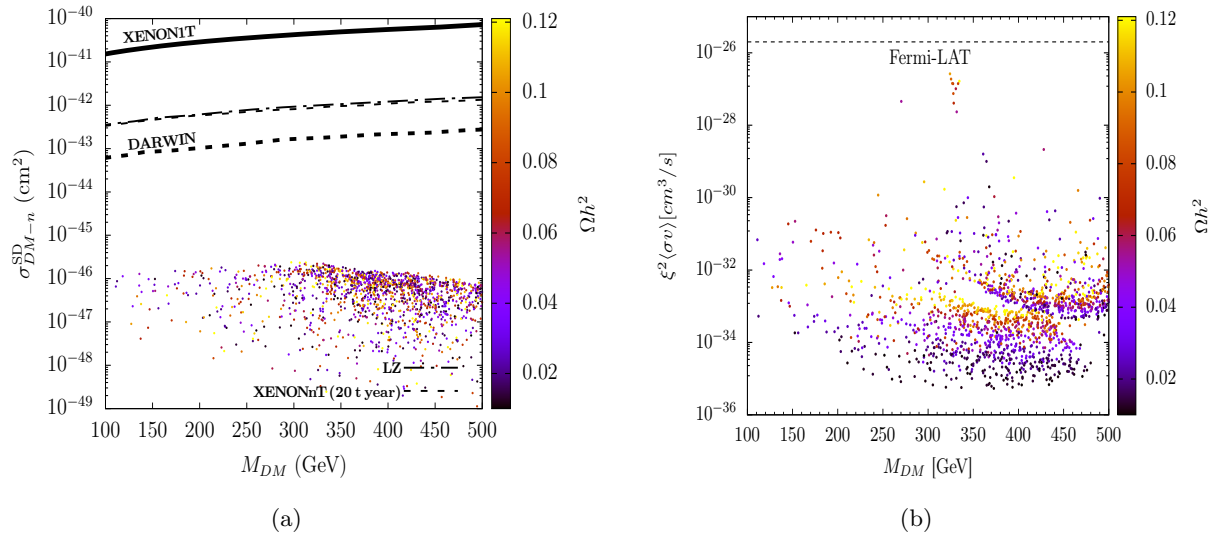


FIG. 9. (a) Scatter plot of spin-dependent cross-section of DM and nucleons. (b) Scatter plot of thermally averaged annihilation cross-section. For both plots, the scan range is set according to Eq. (16).

In the scenario, where the DM (ν_4) and ν_5 have nearly degenerate masses with a mass splitting of $\mathcal{O}(\text{MeV})$, giving them the pseudo-Dirac nature, the $\nu_4\nu_4$ coupling with the Z' becomes very small. While the aforementioned scenarios result in the observed DMRD for $M_{\text{DM}} \in [100, 500]$ GeV, it is also important to check for their signal in the direct detection (DD) experiments. In our scenario we find that the spin-dependent DM-nucleon scattering cross-section measured at the DD experiments is very small. This is because both the Z and Z' coupling to the DM pair is small as mentioned above. Since the mixing angle between the CP-even component of S and H_1 is considered to be less than 10^{-3} , the spin-independent cross-section is also very small due to this minimal scalar mixing. The DM candidate interacts with the neutral gauge bosons Z and Z' through axial vector coupling, resulting in no contribution to the spin-independent DM-nucleon scattering from the gauge boson-mediated channels.

Note that a mass splitting of $\mathcal{O}(10)$ GeV between ν_4 and ν_5 (by setting $Y_L \sim \mathcal{O}(10^{-2})$), increases the spin-dependent cross-section of DM-nucleon interactions. This enhances the detection potential of the DM in DD experiments. The significant mass splitting between ν_4 and ν_5 also suppresses the co-annihilation channel, leading to DM overabundance. For fixed values of $M_{Z'}$, M_{DM} , and M_{ν_5} , the DD cross-section can be enhanced by increasing g_x , though this would alter the dark matter relic density. In Fig. 9(a), we have shown the spin-dependent DM-nucleon cross-section via scatter plot. The points shown in the figure satisfy the DMRD, θ' constraint, DD and indirect detection cross-section bound. From the DD experiments, the bounds on the DM-nucleon cross-section comes

from XENON1T experiment [8, 9]. This upper limit on the cross-section has been shown in Fig. 9(a), and the parameter points are clearly well below the upper limit. The plot also shows the projected sensitivity for several upcoming DM direct detection experiments, such as DARWIN [60], LZ [61], and XENONnT[62].

Indirect detection of DM involves observing visible particles resulting from DM annihilation. The Fermi-LAT and MAGIC [63, 64] collaborations consider $\text{DM DM} \rightarrow b\bar{b}$ and $\text{DM DM} \rightarrow \tau\bar{\tau}$ channels to constrain the thermal average annihilation cross section times relative velocity between two DM particles denoted by $\langle\sigma v\rangle$. The DM annihilation scales with the square of local DM density, $\xi = \frac{\Omega_{\text{DM}}}{0.12}$ [65]. Thus, we have shown $\xi^2\langle\sigma v\rangle$ as a function of DM mass and its RD, along with the Fermi-LAT bound at $\langle\sigma v\rangle = 2 \times 10^{-26} \text{ cm}^3/\text{s}$ in Fig. 9(b). In the scenario with sizeable GKM, the co-annihilation of ν_4 and ν_5 to the SM particles via Z' resonance is the most dominant channel in obtaining DMRD, resulting in a small number of visible particles from DM-DM annihilation. In the singlet scalar resonance region, DM primarily annihilates to $Z'Z'$. To increase DM annihilation to $\tau\bar{\tau}$ and $b\bar{b}$, we need to enhance the singlet scalar's mixing with the SM Higgs.

IV. FIMP SCENARIO

Searches for thermal DM have been going on for more than a decade, and so far, we do not have any observations confirming the nature of DM. Consequently, alternative scenarios that can explain the observed DMRD are being explored. A scenario thus arises, when a DM candidate has a non-thermal nature that leads to non-thermal production of the observed DMRD. These DM candidates have very tiny coupling strengths with visible sector and can easily escape the direct and indirect detection bounds. Particles that show this kind of properties are the so-called FIMPs.

In the non-thermal production mechanism, it is assumed that the particles, which are out of thermal equilibrium, have a very negligible initial abundance and have a feeble interaction with the thermal bath particle. The DM candidates, in this case, are produced from the bath particles via $2 \rightarrow 2$ scattering processes and from the decay of any bath particle to the dark sector. Additionally, BSM particles which are not in equilibrium may decay into dark sector particles. As the DM candidate has negligible initial abundance, the reverse process remains insignificant. Therefore, the DMRD is generated from zero to its current value. This scenario is thus called the freeze-in mechanism.

This is in contrast to the WIMP scenario, where the DM remains in the thermal bath until it freezes out. In the WIMP scenario, increased coupling to thermal bath particles keeps DM in

equilibrium longer and increases annihilation to bath particles, thereby reducing the total yield in the relic density. On the contrary, in the FIMP scenario, as the DM candidate is not in thermal equilibrium with the bath particles, increasing its coupling with bath particles leads to more DM production. Hence, it will increase the total DMRD in the FIMP scenario. One can then easily infer that the coupling should always be below a certain threshold value above which it can enter into the thermal bath. For a particle to be out of equilibrium throughout the evolution of the universe, the rate of conversion of bath particles to the DM particle must remain negligible compared to the Hubble expansion rate.

In a $B_1 B_2 \rightarrow Y \rightarrow X X'$ process, when the s -channel resonance through particle Y occurs, the cross-section of this process can be written as [53]

$$\sigma(s) = \frac{g_Y}{g_{B_1} g_{B_2}} \frac{1}{C_{B_1 B_2}} \frac{4\pi^2 m_Y}{(p_{B_1, B_2}^{\text{CM}})^2} \frac{\Gamma_{Y \rightarrow B_1 B_2} \times \Gamma_{Y \rightarrow X X'}}{\Gamma_{\text{tot.}}} \delta(s - m_Y^2), \quad (20)$$

where g_i is the number of degrees of freedom of the i^{th} initial particle, $p_{1,2}^{\text{CM}}$ are the momenta of initial particles at the centre of mass frame and $s = (p_{B_1}^{\text{CM}} + p_{B_2}^{\text{CM}})^2$. The Γ 's are the partial decay widths of Y in the respective channels and $\Gamma_{\text{tot.}}$ is its total decay width. The factor $C_{B_1 B_2}$ is the combinatorial factor, equals to $\frac{1}{2}$ if two particles are identical otherwise it is equal to 1. Ignoring the back process, the collision term of the Boltzmann equation (see Eq. (14)) at temperature T can be written as [53]

$$R(B_1 B_2 \rightarrow Y \rightarrow X X') = \frac{T g_Y}{2\pi^2} m_Y^2 \frac{\Gamma_{Y \rightarrow B_1 B_2} \times \Gamma_{Y \rightarrow X X'}}{\Gamma_{\text{tot.}}} \tilde{K}_1(x_Y, x_1, x_2, 0, \eta_1, \eta_2), \quad (21)$$

where, for i^{th} particle, $x_i = m_i/T$ and $\eta_i = \pm e^{\mu_i/T}$ for bosons/fermions (+/-) with chemical potential μ_i . The function \tilde{K}_1 is given by [53]

$$\tilde{K}_1(x_1, x_2, x_3, \eta_1, \eta_2, \eta_3) = \frac{1}{16\pi^2 p_{1,2}^{\text{CM}} T} \int \prod_{i=1}^3 \left(\frac{d^3 p_i}{E_i} \frac{1}{e^{E_i/T} - \eta_i} \right) e^{E_1/T} \delta^4(p_1 - p_2 - p_3). \quad (22)$$

In the standard FIMP scenario, the evolution of the DM density begins after the reheating phase. During this phase the inflaton field decays, creating a thermal bath, from which the non thermal DM is generated. Throughout the analysis, we have kept the reheating temperature T_R to be 10^{10} GeV. We work in the regime where the mediator that produces DM from its decay has a mass much smaller than the reheating temperature. The DMRD is very much unaffected by variation of reheating temperature unless it is close to the mediator mass [35, 66].

As mentioned previously, in this work, we consider the lightest heavy right-handed neutrino (ν_4) as a possible DM candidate. In the WIMP scenario, we have already seen that ν_4 can be stable

because of its small Yukawa couplings ($Y_{\nu_{11}} = 10^{-27}$ and $Y_{\nu_{12}} = 0 = Y_{\nu_{13}}$). In the FIMP scenario however, the couplings, g_x and $Y_{L_{11}}$ must be small enough to keep ν_4 out of thermal bath. Additionally the couplings should not be very small such that the observed DMRD cannot be achieved.

In the WIMP scenario, we have seen that there is a small mass difference between ν_4 and ν_5 . Being the lightest, the ν_4 is stable, and ν_5 decays to ν_4 and a pair of SM fermions via the exchange of off-shell Z , Z' or h_s . In the FIMP scenario, due to small values of g_x and $Y_{L_{11}}$, ν_5 can be a long-lived particle. If both Z' and h_s are out of thermal equilibrium, the lifetime of ν_5 can be larger than the age of the universe as the GKM and the singlet scalar mixing angles with other scalars are very small. In order to avoid this additional DM component, we have chosen the value of $v_s Y_{L_{11}}$ (see Eq. (11)) such that it creates a mass difference between ν_4 and ν_5 large enough to make the decay $\nu_5 \rightarrow \nu_4 Z' / \nu_4 h_s$ kinematically possible.

Some points to note about the other particles, *viz.* the heavy neutrinos ($\nu_6, \nu_7, \nu_8, \nu_9$) will be in the thermal bath because of their sizeable coupling with the second Higgs doublet and SM neutrinos. Similarly the scalars A, h_2 and H^\pm are in thermal equilibrium as they couple to the SM gauge bosons with electroweak strength. Since the DM (ν_4) interacts only with Z' and h_s it can be produced from their exchange as well as decay. The production of the DM can happen when the Z' and h_s are either in thermal equilibrium or out of thermal equilibrium. We shall consider both these scenarios for DM production in the following subsections.

A. The DM production via Z'

In this section, we consider DM production through the decay or exchange of Z' only while keeping h_s out of thermal equilibrium with negligible coupling to the DM. The Z' interacts with the SM particles via GKM (g'_x) and its mixing with the SM Z -boson (θ'). As the DM is out of the thermal bath, its couplings including the $U(1)_X$ gauge coupling g_x must be very small. As a result, the interaction of Z' with heavy neutrinos becomes weak. So g'_x and θ' will determine whether the Z' will remain in the thermal bath. Thus, two distinct cases emerge where (a) the Z' is out of thermal equilibrium, and, (b) the Z' is in thermal equilibrium.

We find that the DM candidate (ν_4) becomes non-thermal for $g_x < 10^{-9}$ and $Y_{L_{11}} < 10^{-9}$. This range of g_x makes Z' very light unless the $U(1)_X$ symmetry breaking scale, v_s is chosen to be very large. We set $v_s \sim \mathcal{O}(10^{13})$ GeV to achieve a Z' mass within the range of a few GeV to a few TeV. As the couplings and mixings involved here are very small, the Z' mass is easily

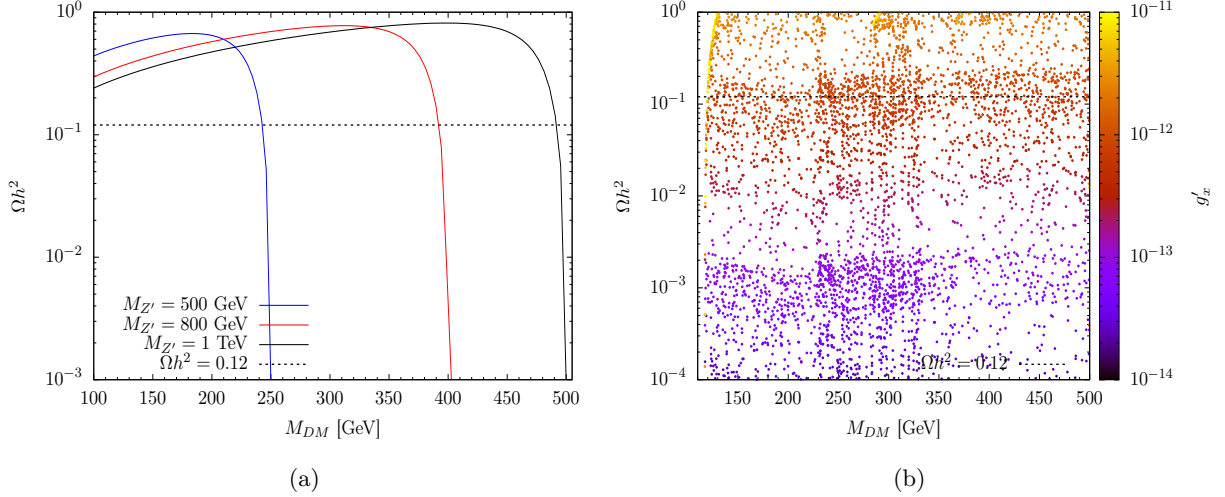


FIG. 10. (a) The DMRD Ωh^2 versus M_{DM} for $M_{Z'} = 500, 800, 1000$ GeV at $g'_x = 2 \times 10^{-12}$. (b) Scatter plot presenting the DMRD Ωh^2 as a function of M_{DM} and g'_x .

allowed by the constraints obtained from Z' searches (Drell-Yan) at the LHC [67–69]. We vary $g'_x \in [10^{-14}, 10^{-11}]$ that keeps Z' out of thermal equilibrium. In addition, the scalar mixing matrix elements Z_{13}^h, Z_{23}^h are chosen in the range of $\mathcal{O}(10^{-15} - 10^{-10})$ and $Y_{L22} \simeq Y_{L33} \simeq \mathcal{O}(10^{-11})$ to ensure that the singlet scalar h_s never attains thermal equilibrium. In this scenario, we fix all the remaining heavy neutrino masses beyond ν_5 to be $m_{\nu_H} \simeq 4$ TeV. The scalar sector values are chosen as $M_{h_2} = M_A = M_{H^\pm} = 1.5$ TeV, $\tan \beta = 10^{-4}$ and $v_s = 10^{13}$ GeV.

In Fig. 10(a), we show the DMRD (Ωh^2) as a function of the DM mass M_{DM} for three different values of $M_{Z'}$ with a fixed value of $g'_x = 2 \times 10^{-12}$. Here, we see that the observed DMRD can be achieved near $M_{Z'} \simeq 2M_{DM}$. In the overabundant region the correct relic can be achieved by varying the GKM. The figure clearly shows a sharp drop in DMRD when M_{DM} exceeds $M_{Z'}/2$, indicating that for $M_{DM} > M_{Z'}/2$, the off-shell production of Z' contributes negligibly to the DMRD. In the present scenario, since the GKM is non-zero, reversing the channels that contribute to the DMRD in the WIMP section under a non-zero GKM condition assists in achieving the correct relic density for the FIMP. The dominant DM production channels are $f\bar{f} \rightarrow Z' \rightarrow \nu_4\nu_4$, $W^+W^- \rightarrow Z' \rightarrow \nu_4\nu_4$, and $h_1Z \rightarrow Z' \rightarrow \nu_4\nu_4$. The DM production due to the heavy neutrinos annihilation via an offshell Z' is negligible since $m_{\nu_H} \simeq 4$ TeV $\gg M_{Z'}$. To suppress the DM production from the singlet-dominated CP-even scalar in the Z' driven scenario, we keep h_s lighter than the heavy neutrinos and the corresponding scalar sector mixing angles very small.

In the region where $2M_{DM} < M_{\text{mediator}} < T_R$, the dominant contribution to the DM production

occurs when the centre-of-mass energy \sqrt{s} is approximately equal to M_{mediator} (see Eq. (20)). In this region the final DMRD is relatively insensitive to T_R [66]. In Fig. 10(a), we have considered three benchmark points (BPs) with three values of $M_{Z'}$. We find when there is enough phase space available for Z' to decay into a pair of DMs, the BP with lightest Z' yield in largest DMRD. Which can be explained as follows, referring to equation (21) the magnitude of $\Gamma_{Z' \rightarrow \text{SM}} \text{SM} \times \text{BR}_{Z' \rightarrow \text{DM}} \text{DM}$ is higher for larger masses of Z' for given value for DM mass and the temperature-dependent function \tilde{K}_1 is more significant for lighter masses of Z' . Consequently, the DM production is maximised when $M_{Z'}$ is heaviest until the temperature of the universe matches the Z' mass. However, as the temperature T drops below the mediator mass, the production of DM from bath particles is considerably more suppressed for a heavy mediator compared to a lighter one. Thus, for $T < 500$ GeV, the BP with $M_{Z'} = 500$ GeV yields more DM compared to the other two BPs, resulting in the highest RD for a given M_{DM} , if there much phase space available for Z' decay to a DM pair.

In Fig. 10(b), we show the variation of Ωh^2 as a function of the DM mass and the GKM. In this scatter plot, we vary $M_{\text{DM}} \in [100, 500]$ GeV, $M_{Z'} \in [100, 1000]$ GeV and $g'_x \in [10^{-14}, 10^{-11}]$. We find that the observed DMRD can be obtained for $g'_x \simeq \mathcal{O}(10^{-12})$. For the higher values of the GKM ($> 10^{-12}$), the coupling of Z' to the SM particles becomes stronger, which leads to an overabundance of the DMRD. Similarly, the smaller values of the GKM ($< 10^{-12}$) would give under-abundant DMRD.

Now, we explore the case where Z' is in thermal equilibrium, achieved by making the GKM g'_x large while keeping $\theta' < 10^{-3}$. In this region, we achieve the correct DMRD mainly through two processes: (a) via Z' decay and (b) via h_s resonance through $Z'Z'$ and ZZ annihilation processes. We will discuss the h_s resonance process in the next subsection.

In Fig. 11, we show the DMRD for two different masses of Z' . The observed DMRD can be obtained when a pair of DM is produced from decay of Z' . The black and red solid curves, respectively, are for $M_{Z'} = 500$ GeV and $M_{Z'} = 800$ GeV with $g'_x = 5 \times 10^{-4}$. The blue dashed curve is for $M_{Z'} = 800$ GeV with $g'_x = 5 \times 10^{-5}$. The red solid and blue dashed curves are overlapping although the red curve has one order of magnitude larger GKM as compared to the blue dashed curve. This demonstrates that varying the GKM does not significantly alter the DMRD as long as Z' is in the thermal bath. This is because, the branching ratio (BR) of Z' to SM particles is close to one. The production of non-thermal particles from the decay of a thermal bath particle depends on its partial decay width to that mode [53]. Therefore, the distribution of DMRD remains similar for these two BPs. Finally, the black curve with $M_{Z'} = 500$ GeV shows a smaller Ωh^2 compared

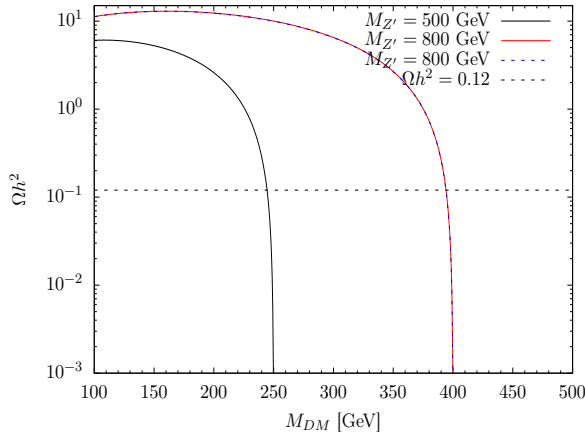


FIG. 11. Variation of the DMRD as a function of the DM mass when Z' is in thermal equilibrium.

to the blue and red curves with $M_{Z'} = 800$ GeV. This is because, for a given DM mass, the partial decay width of a heavier Z' to a DM pair is larger, as it is proportional to g_x^3 .

B. The DM production via h_s

As the DM candidate couples to the singlet scalar h_s via the Yukawa coupling Y_{L11} , it can potentially be produced from h_s decay. In such scenarios, we have two cases: (a) h_s is out of thermal equilibrium, and (b) h_s is in thermal equilibrium. Note that in this subsection the Z' contribution to the DM production is negligible due to our assumption that $M_{Z'} < 2M_{\text{DM}}$. The mixing angles, governed by the quartic couplings λ_{1s} and λ_{2s} are responsible for keeping the singlet scalar h_s in the thermal bath. In this subsection, we fix $m_{\nu_H} \simeq 4$ TeV, $M_{h_2} = M_A = M_{H^\pm} = 1.5$ TeV, $M_{Z'} = 100$ GeV, $\tan \beta = 10^{-4}$ and $v_s = 10^{13}$ GeV.

We first consider the non-thermal h_s case. In this case, h_s can be produced from the thermal bath via two types of processes: (i) from the SM particles due to the mixing of singlet scalar with other CP-even scalars, and (ii) from the non-SM particles such as the heavy neutrinos ν_H and the thermal Z' . In the first scenario, we set $\lambda_{1s} \in [10^{-24}, 10^{-19}]$, $\lambda_{2s} = 0$ and $Y_{L11} = 8.5 \times 10^{-11}$, which generate non-zero small mixing between h_s and the other scalars.³ The mixing angle of the singlet scalar with the SM-like Higgs h_1 is very small ($Z_{13}^h = \mathcal{O}(10^{-15} - 10^{-10})$), while the mixing angle with h_2 is even more suppressed than Z_{13}^h due to $\lambda_{2s} = 0$. The singlet scalar h_s is kept lighter than the heavy neutrinos, preventing its single on-shell production from them. The dominant

³ In this study, λ_{2s} is fixed at zero, as by considering a non-zero λ_{2s} this does not add any new processes for the h_s production from the thermal bath. Moreover, the coupling strength of h_2 to the SM particles is $\tan \beta$ suppressed.

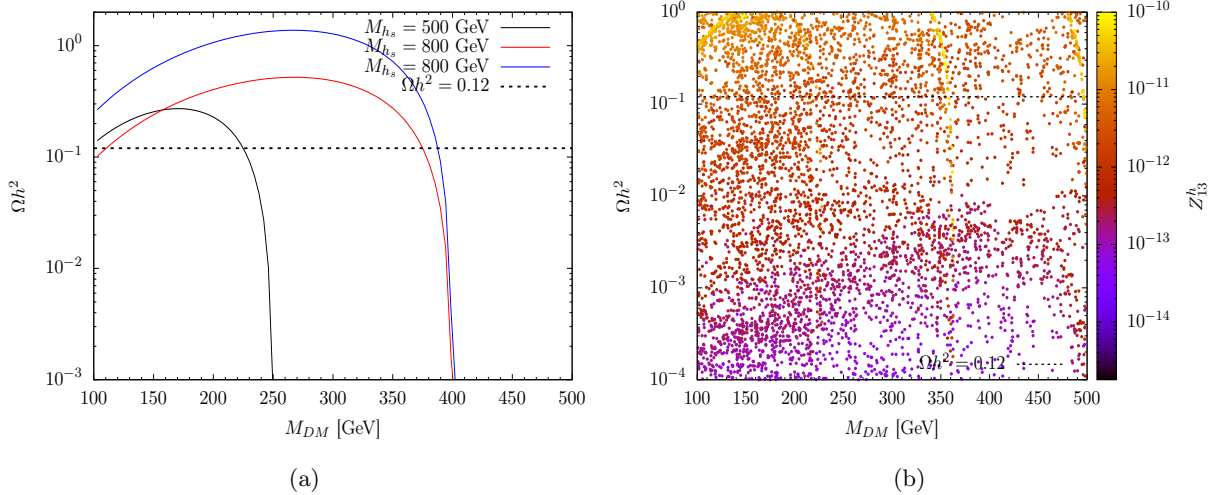


FIG. 12. (a) The DMRD Ωh^2 versus M_{DM} for $M_{h_s} = 500, 800$ GeV. (b) Scatter plot presenting the DMRD Ωh^2 as a function of M_{DM} and Z^h_{13} . In both panels, $M_{Z'} = 100$ GeV.

channels for the DM production are $W^+W^-/h_1h_1/ZZ/t\bar{t} \rightarrow h_s \rightarrow DM DM$. In Fig. 12(a), we show the variation of Ωh^2 as a function of the DM mass. In this figure, the black curve represents $M_{h_s} = 500$ GeV, and the blue and red curves represent $M_{h_s} = 800$ GeV. For the black and red curves $Z^h_{13} = 5.0 \times 10^{-12}$ while for the blue curve $Z^h_{13} \simeq 10^{-11}$. The distribution of relic density shows that the DM production is significant when h_s is produced on-shell and then decays to a DM pair. When $M_{DM} > M_{h_s}/2$ the DM pair production is now away from the h_s resonance and therefore the contribution from the off-shell h_s becomes negligible. Initially, the DMRD grows with increasing DM mass because the energy density is a monotonically increasing function of the DM mass. However, due to phase space suppression (as the DM mass approaches $M_{h_s}/2$) the production rate drops, resulting in the decrease of DMRD. As in the case of Z' , here too we observe that the DMRD can be satisfied when the h_s is produced on-shell from the thermal bath and decays to a pair of DM. In the overabundant region, the observed DMRD can be satisfied by varying Z^h_{13} . Although both the blue and the red curves correspond to the same value of M_{h_s} , they differ in the DMRD because of the difference in mixing angle of h_s with the SM-like Higgs. The blue curve, having a larger mixing angle Z^h_{13} , results in more h_s production from the thermal bath, thereby yielding a larger DMRD. In Fig. 12(b), a scatter plot shows the DMRD as a function of M_{DM} and Z^h_{13} . In this scatter plot, we scan over the relevant parameters in the following range

$$M_{DM} \in [100, 500] \text{ GeV}, \quad M_{h_s} \in [100, 3500] \text{ GeV}, \quad \text{and} \quad Z^h_{13} \in [10^{-14}, 10^{-10}].$$

We find that the correct DMRD can be achieved for the whole range of M_{DM} in this scan with

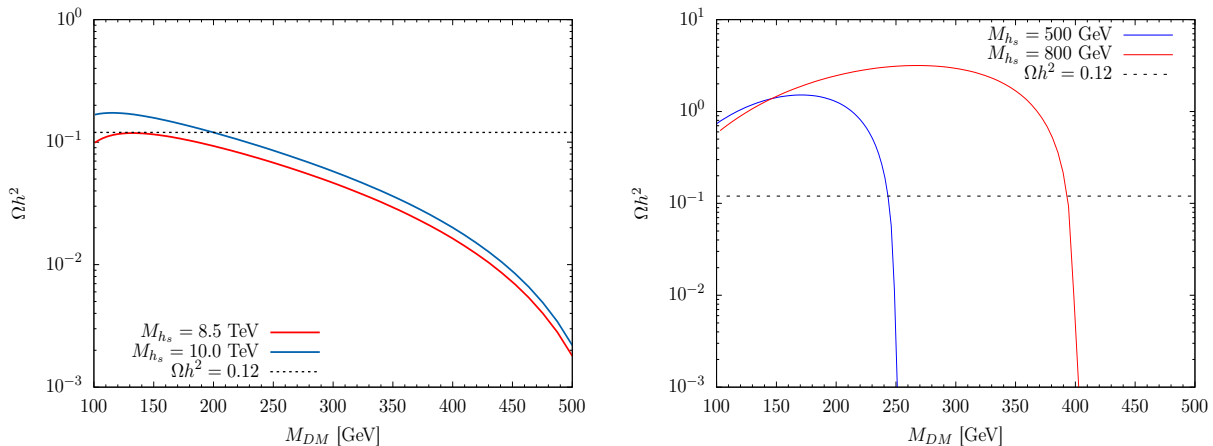


FIG. 13. Variation of the DMRD versus M_{DM} for a non-thermal h_s production from heavy neutrinos annihilation (left panel) and $Z'Z'$ annihilation (right panel). Here, $M_{Z'} = 100$ GeV and the masses of four heavy neutrinos are 3.4 TeV, 3.9 TeV, 4.1 TeV, and 4.7 TeV.

$Z_{13}^h \in [10^{-12}, 10^{-11}]$, as shown in the figure palette.

In the scenario with vanishing scalar mixing, where the singlet scalar cannot be produced from SM particles, its production relies on pair of heavy neutrino annihilation and Z' annihilation. For the processes $\nu_i \nu_j \rightarrow h_s \rightarrow \nu_4 \nu_4$ ⁴ where $i, j = 6 - 9$, the h_s mass is chosen such that it would be heavier than the sum of the masses of any two heavy neutrinos, so the scalar can be produced from their annihilation. In Fig. 13 (left panel), we show the variation of Ωh^2 as a function of M_{DM} for two different values of $M_{h_s} = 8.5, 10$ TeV. In this figure, we vary $Y_{L11} \in [8 \times 10^{-12}, 2 \times 10^{-10}]$ to keep $M_{DM} \in [100, 500]$ GeV and fix $Y_{L22} = 1.6 \times 10^{-11}$, $Y_{L33} = 9.4 \times 10^{-11}$. For $M_{h_s} = 8.5$ TeV, the production of h_s from the heaviest heavy neutrinos is kinematically forbidden, resulting in a slightly smaller DMRD compared to $M_{h_s} = 10$ TeV.

For the process $Z'Z' \rightarrow h_s \rightarrow \nu_4 \nu_4$, where Z' is in thermal equilibrium but cannot produce a DM pair (i.e., $M_{Z'} < 2M_{DM}$), there is a possibility of achieving the correct DMRD via singlet scalar resonance if it is feasible kinematically. In Fig. 13 (right panel), we plot Ωh^2 as a function of M_{DM} for two different values of M_{h_s} , fixing $g'_x = 10^{-4}$ and $Y_{L11} = 8.5 \times 10^{-11}$. Here, again we see that the correct DMRD can be satisfied when $M_{DM} < M_{h_s}/2$.

Now, we consider the second case where h_s is in thermal equilibrium. The singlet scalar h_s will be in thermal equilibrium if it has large enough mixing with the other CP even scalar components. For example, a mixing of $Z_{13}^h \simeq \mathcal{O}(10^{-4})$ is large enough for the h_s to remain in thermal equilibrium

⁴ The contribution of $\nu_\ell \nu_\ell \rightarrow h_s \rightarrow \nu_4 \nu_4$ to the DMRD is very small because the heavy neutrinos ν_H have small mixings with the active ones (ν_ℓ).

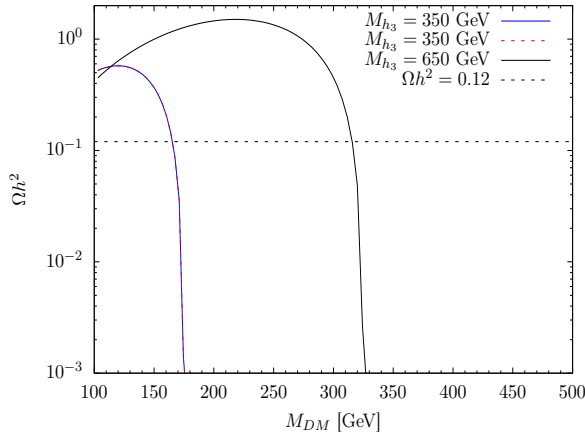


FIG. 14. Variation of the DMRD as a function of the DM mass when h_s is in thermal equilibrium.

with the bath particles. Note that very large values of $Z_{13}^h \gtrsim 10^{-2}$ is likely to get constrained from the SM Higgs measurements at the LHC [70]. In Fig. 14, we show the DMRD as a function of M_{DM} . The blue and black curves correspond to $M_{h_s} = 350$ GeV and $M_{h_s} = 650$ GeV, respectively, with $Z_{13}^h \simeq 9 \times 10^{-4}$. In this figure, we find that the observed DMRD is achievable in the region $M_{\text{DM}} < M_{h_s}/2$. The rapid fall in the DMRD for $M_{\text{DM}} > M_{h_s}/2$ shows its production is via off-shell h_s . The red dashed curve is also with $M_{h_s} = 350$ GeV but with a different value of $Z_{13}^h \simeq 9 \times 10^{-5}$. The blue curve has one order larger coupling strength with the SM particles as compared to the red curve. However, both of them give the same amount of the DMRD. The reason is similar to the case discussed in the previous section for the thermal Z' -boson scenario.

V. SUMMARY AND CONCLUSION

In this article, we consider a $U(1)$ extension of the SM gauge symmetry, where the SM particles are singlet under this newly added abelian gauge symmetry. This model includes an additional doublet scalar, three vector-like SM gauge singlet fermions, and a singlet scalar, all charged under the new $U(1)$ gauge group. The new singlet and doublet scalars are responsible for the spontaneous breaking of the new gauge symmetry. The second Higgs doublet and the SM singlet fermions couple to SM leptons with a Yukawa coupling. Due to this interaction term, the SM neutrinos become massive at tree level when the second Higgs doublet acquires a vev. In this work we assume that the lightest of the heavy neutrinos acts as the DM candidate. To make this happen, we require that the coupling of the lightest of the heavy neutrinos (Y_ν) must be smaller than $\mathcal{O}(10^{-27})$ so that

its lifetime becomes larger than the age of the universe. We have studied the viability of both the WIMP and FIMP mechanisms in this model to achieve the observed DMRD.

When the DM is thermal, its RD can be achieved via Z' mediated (co)annihilation channels if GKM and Z - Z' mixing angle are non-negligible. If these parameters are vanishingly small, the correct DMRD can be obtained through s -channel singlet scalar resonance. The scenario where the singlet scalar and Z' are lighter than the DM, the observed DMRD is achieved when the DM annihilates to h_s and Z' in the final state. The non-thermal DM can be obtained by making all its interactions with particles in the thermal bath feeble. We consider both thermal and non-thermal nature of the new gauge boson Z' and the singlet scalar h_s to show how these affect the DM production, when they mediate the interaction between DM and visible sector.

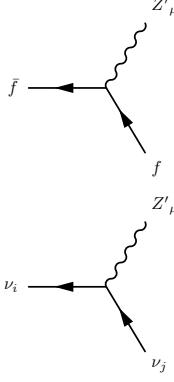
The study in this work sheds light on the distinctive feature of having DM candidates within the framework of the neutrinophilic $U(1)$ model and thereby contributes to the ongoing discourse of DM candidates. The study aims to broaden the area of phenomenological aspects of the neutrinophilic model, which has already been studied in a wide range of aspects including collider signals, neutrino mass and mixings, and its role in lepton flavour violating signals. Future directions include an exploration of the phenomenological study of light DM between mass range $\mathcal{O}(\text{keV} - \text{GeV})$. Notably, the future study would also focus on how thermal correction to masses and couplings affect the feasible DM parameter space as well as the possible collider studies of the DM in this model.

ACKNOWLEDGMENTS

AKB and SKR would like to acknowledge the support from the Department of Atomic Energy (DAE), India, for the Regional Centre for Accelerator-based Particle Physics (RECAPP), Harish Chandra Research Institute. TS thanks ICTS, Bengaluru and IISc, Bengaluru, for their hospitality when part of this work was being carried out.

Appendix A: Feynman rules

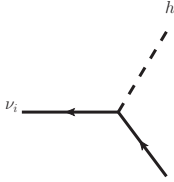
Below, we outline the relevant couplings of the model. We define $s_W \equiv \sin \theta_W$ and $c_W \equiv \cos \theta_W$, where θ_W is the Weinberg angle. Similarly, define $s_{\theta'} \equiv \sin \theta'$ and $c_{\theta'} \equiv \cos \theta'$, where θ' is the Z - Z' mixing angle. Additionally, T_3 denotes the isospin, and Q_f represents the electric charge of the fermions. The projection operators are given by $P_{L/R} = \frac{1 \mp \gamma_5}{2}$.



The first diagram shows a fermion \bar{f} and a fermion f interacting via a Z'_μ boson. The second diagram shows a neutrino ν_i and a neutrino ν_j interacting via a Z'_μ boson.

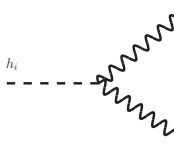
$$\begin{aligned}
& i \left(\frac{e s_{\theta'}}{s_W c_W} (T^3 - Q_f s_W^2) + g'_x c_{\theta'} (T^3 - Q_f) \right) \gamma^\mu P_L - i \left(\frac{e s_{\theta'}}{s_W c_W} Q_f s_W^2 + g'_x c_{\theta'} Q_f \right) \gamma^\mu P_R \\
& \frac{i}{2} \left(\left(\frac{e s_{\theta'}}{2 s_W c_W} + \frac{g'_x}{2} c_{\theta'} \right) \sum_{k=1}^3 \mathcal{N}_{ik} \mathcal{N}_{jk}^* - g_x c_{\theta'} \left(- \sum_{k=7}^9 \mathcal{N}_{ik} \mathcal{N}_{jk}^* + \sum_{k=4}^6 \mathcal{N}_{ik} \mathcal{N}_{jk}^* \right) \right) \gamma^\mu P_L \\
& - \frac{i}{2} \left(\left(\frac{e s_{\theta'}}{2 s_W c_W} + \frac{g'_x}{2} c_{\theta'} \right) \sum_{k=1}^3 \mathcal{N}_{ik}^* \mathcal{N}_{jk} - g_x c_{\theta'} \left(- \sum_{k=7}^9 \mathcal{N}_{ik}^* \mathcal{N}_{jk} + \sum_{k=4}^6 \mathcal{N}_{ik}^* \mathcal{N}_{jk} \right) \right) \gamma^\mu P_R,
\end{aligned}$$

where \mathcal{N} is the neutrino mixing matrix. We note that ν_i for $i = 1, 2, 3$ are identified as the light neutrinos and rest are heavy neutrinos. These neutrinos are Majorana fermions written in 4-component notation.



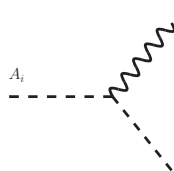
The diagram shows a neutrino ν_i and a neutrino ν_j interacting via a scalar boson h_k .

$$- \frac{i}{\sqrt{2}} \left(\sum_{a=1}^3 \sum_{b=1}^3 \mathcal{N}_{i6+a}^* \mathcal{N}_{j6+b} Y_{Lab} \right) Z_{h_{k3}} P_L - \frac{i}{\sqrt{2}} \left(\sum_{a=1}^3 \sum_{b=1}^3 \mathcal{N}_{i6+a} \mathcal{N}_{j6+b} Y_{Lab}^* \right) Z_{h_{k3}} P_R$$



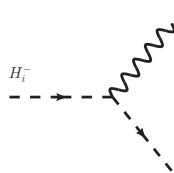
The diagram shows a neutrino h_i and a neutrino h_j interacting via Z_μ and Z'_μ bosons.

$$\begin{aligned}
& \frac{i}{2} \left(v_1 \left((g_1 s_W + g_2 c_W) s_{\theta'} + g'_x c_{\theta'} \right)^2 Z_{h_{i1}} + v_2 \left((2g_x + g'_x) c_{\theta'} \right. \right. \\
& \left. \left. + (g_1 s_W + g_2 c_W) s_{\theta'} \right)^2 Z_{h_{i2}} + 16v_s (g_x c_{\theta'})^2 Z_{h_{i3}} \right) g_{\sigma\mu}
\end{aligned}$$



The diagram shows a neutrino A_i and a neutrino h_j interacting via a Z'_μ boson and charged scalars.

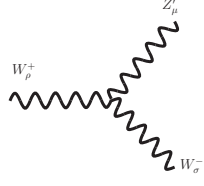
$$\begin{aligned}
& - \frac{1}{2} \left((g_1 s_W + g_2 c_W) s_{\theta'} + g'_x c_{\theta'} \right) Z_{A_{i1}} Z_{h_{j1}} + \left((2g_x + g'_x) c_{\theta'} \right. \\
& \left. + (g_1 s_W + g_2 c_W) s_{\theta'} \right) Z_{A_{i2}} Z_{h_{j2}} - 4g_x c_{\theta'} Z_{A_{i3}} Z_{h_{j3}} \left(p_\mu^{A_i} - p_\mu^{h_j} \right)
\end{aligned}$$



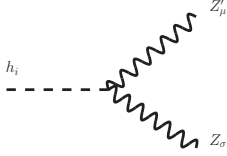
The diagram shows a neutrino H_i^- and a neutrino H_j^+ interacting via a Z'_μ boson and charged scalars.

$$\begin{aligned}
& \frac{i}{2} \left((g_1 s_W - g_2 c_W) s_{\theta'} + g'_x c_{\theta'} \right) Z_{C_{i1}} Z_{C_{j1}} + \left((2g_x + g'_x) c_{\theta'} \right. \\
& \left. + (g_1 s_W - g_2 c_W) s_{\theta'} \right) Z_{C_{i2}} Z_{C_{j2}} \left(p_\mu^{H_i^-} - p_\mu^{H_j^+} \right)
\end{aligned}$$

Here, Z_h , Z_A and Z_C are mixing matrices for CP-even, CP-odd, and charged scalars, respectively.



$$i g_2 c_W s_{\theta'} \left(g_{\rho\mu} \left(-p_{\sigma}^{Z'\mu} + p_{\sigma}^{W_{\rho}^+} \right) + g_{\rho\sigma} \left(-p_{\mu}^{W_{\rho}^+} + p_{\mu}^{W_{\rho}^-} \right) + g_{\sigma\mu} \left(-p_{\rho}^{W_{\rho}^-} + p_{\rho}^{Z'\mu} \right) \right)$$



$$\begin{aligned} & \frac{i}{4} \left(v_1 \left(-2g'_x g_2 c_W c_{2\theta'} - 2g_1 g'_x c_{\theta'}^2 s_W + 2g_1 g'_x s_W s_{\theta'}^2 \right. \right. \\ & \quad \left. \left. + g'_x{}^2 s_{2\theta'} - g_2^2 c_{\theta'}^2 s_{2\theta'} - g_1^2 s_W^2 s_{2\theta'} - g_1 g_2 s_{2W} s_{2\theta'} \right) Z_{h_{i1}} \right. \\ & \quad \left. - v_2 \left(g_2 c_W \left(2 \left(2g_x + g'_x \right) c_{2\theta'} - g_1 c_{2\theta'+\theta_W} + g_1 c_{2\theta'-\theta_W} \right) \right. \right. \\ & \quad \left. \left. + 2g_1 \left(2g_x + g'_x \right) c_{\theta'}^2 s_W + 2s_W s_{\theta'} \left(g_1 \left(- \left(2g_x + g'_x \right) s_{\theta'} + g_1 c_{\theta'} s_W \right) \right) \right. \right. \\ & \quad \left. \left. - \left(2g_x + g'_x \right)^2 s_{2\theta'} + g_2^2 c_{\theta'}^2 s_{2\theta'} \right) Z_{h_{i2}} + 16v_S \left(-g_x^2 s_W^2 \right) Z_{h_{i3}} \right) \left(g_{\sigma\mu} \right) \end{aligned}$$

- [1] F. Zwicky, *Helv. Phys. Acta* **6**, 110 (1933).
- [2] H. W. Babcock, *Lick Observatory Bulletin* **498**, 41 (1939).
- [3] V. C. Rubin, J. Ford, W. K., and N. Thonnard, *Astrophys. J.* **238**, 471 (1980).
- [4] R. Massey, T. Kitching, and J. Richard, *Rept. Prog. Phys.* **73**, 086901 (2010), arXiv:1001.1739 [astro-ph.CO].
- [5] D. Clowe, M. Bradac, A. H. Gonzalez, M. Markevitch, S. W. Randall, C. Jones, and D. Zaritsky, *Astrophys. J. Lett.* **648**, L109 (2006), arXiv:astro-ph/0608407.
- [6] C. L. Bennett *et al.* (WMAP), *Astrophys. J. Suppl.* **208**, 20 (2013), arXiv:1212.5225 [astro-ph.CO].
- [7] N. Aghanim *et al.* (Planck), *Astron. Astrophys.* **641**, A6 (2020), [Erratum: *Astron. Astrophys.* 652, C4 (2021)], arXiv:1807.06209 [astro-ph.CO].
- [8] E. Aprile *et al.* (XENON), *Phys. Rev. Lett.* **121**, 111302 (2018), arXiv:1805.12562 [astro-ph.CO].
- [9] E. Aprile *et al.* (XENON), *Phys. Rev. Lett.* **122**, 141301 (2019), arXiv:1902.03234 [astro-ph.CO].
- [10] Y. Meng *et al.* (PandaX-4T), (2021), arXiv:2107.13438 [hep-ex].
- [11] E. W. Kolb and M. S. Turner, *The Early Universe*, Vol. 69 (1990).
- [12] G. Jungman, M. Kamionkowski, and K. Griest, *Phys. Rept.* **267**, 195 (1996), arXiv:hep-ph/9506380.
- [13] G. Bertone, D. Hooper, and J. Silk, *Phys. Rept.* **405**, 279 (2005), arXiv:hep-ph/0404175.
- [14] L. J. Hall, K. Jedamzik, J. March-Russell, and S. M. West, *JHEP* **03**, 080 (2010), arXiv:0911.1120 [hep-ph].
- [15] J. Edsjö and P. Gondolo, *Phys. Rev. D* **56**, 1879 (1997).
- [16] M. Dutra, C. A. de S. Pires, and P. S. Rodrigues da Silva, *JHEP* **09**, 147 (2015), arXiv:1504.07222 [hep-ph].

- [17] J. K. Mizukoshi, C. A. de S. Pires, F. S. Queiroz, and P. S. Rodrigues da Silva, *Phys. Rev. D* **83**, 065024 (2011), [arXiv:1010.4097 \[hep-ph\]](#).
- [18] P. Fayet, (2006), [arXiv:hep-ph/0607094](#).
- [19] H. An, M. Pospelov, J. Pradler, and A. Ritz, *Phys. Lett. B* **747**, 331 (2015), [arXiv:1412.8378 \[hep-ph\]](#).
- [20] M. Pospelov, A. Ritz, and M. B. Voloshin, *Phys. Lett. B* **662**, 53 (2008), [arXiv:0711.4866 \[hep-ph\]](#).
- [21] I. Chakraborty, D. K. Ghosh, N. Ghosh, and S. K. Rai, *Eur. Phys. J. C* **81**, 679 (2021), [arXiv:2104.03351 \[hep-ph\]](#).
- [22] S. Dey, P. Ghosh, and S. K. Rai, *Eur. Phys. J. C* **82**, 876 (2022), [arXiv:2202.11638 \[hep-ph\]](#).
- [23] P. Gondolo and G. Gelmini, *Nucl. Phys. B* **360**, 145 (1991).
- [24] C. E. Yaguna, *JHEP* **08**, 060 (2011), [arXiv:1105.1654 \[hep-ph\]](#).
- [25] X. Chu, T. Hambye, and M. H. G. Tytgat, *JCAP* **05**, 034 (2012), [arXiv:1112.0493 \[hep-ph\]](#).
- [26] B. Shakya, *Mod. Phys. Lett. A* **31**, 1630005 (2016), [arXiv:1512.02751 \[hep-ph\]](#).
- [27] M. Pandey, D. Majumdar, and K. P. Modak, *JCAP* **06**, 023 (2018), [arXiv:1709.05955 \[hep-ph\]](#).
- [28] F. Elahi, C. Kolda, and J. Unwin, *JHEP* **03**, 048 (2015), [arXiv:1410.6157 \[hep-ph\]](#).
- [29] N. Bernal, M. Heikinheimo, T. Tenkanen, K. Tuominen, and V. Vaskonen, *Int. J. Mod. Phys. A* **32**, 1730023 (2017), [arXiv:1706.07442 \[hep-ph\]](#).
- [30] A. Merle, V. Niro, and D. Schmidt, *JCAP* **03**, 028 (2014), [arXiv:1306.3996 \[hep-ph\]](#).
- [31] A. Ghosh, T. Mondal, and B. Mukhopadhyaya, *JHEP* **12**, 136 (2017), [arXiv:1706.06815 \[hep-ph\]](#).
- [32] C. Cosme, M. Dutra, S. Godfrey, and T. R. Gray, *JHEP* **09**, 056 (2021), [arXiv:2104.13937 \[hep-ph\]](#).
- [33] C. Cosme, M. Dutra, T. Ma, Y. Wu, and L. Yang, *JHEP* **03**, 026 (2021), [arXiv:2003.01723 \[hep-ph\]](#).
- [34] G. Bhattacharyya, M. Dutra, Y. Mambrini, and M. Pierre, *Phys. Rev. D* **98**, 035038 (2018), [arXiv:1806.00016 \[hep-ph\]](#).
- [35] W. Abdallah, S. Choubey, and S. Khan, *JHEP* **06**, 095 (2019), [arXiv:1904.10015 \[hep-ph\]](#).
- [36] W. Abdallah, A. K. Barik, S. K. Rai, and T. Samui, (2021), [arXiv:2106.01362 \[hep-ph\]](#).
- [37] R. W. Robinett and J. L. Rosner, *Phys. Rev. D* **25**, 3036 (1982), [Erratum: *Phys.Rev.D* 27, 679 (1983)].
- [38] R. W. Robinett and J. L. Rosner, *Phys. Rev. D* **26**, 2396 (1982).
- [39] P. Langacker, R. W. Robinett, and J. L. Rosner, *Phys. Rev. D* **30**, 1470 (1984).
- [40] J. L. Hewett and T. G. Rizzo, *Phys. Rept.* **183**, 193 (1989).
- [41] W. Abdallah, A. K. Barik, S. K. Rai, and T. Samui, *Phys. Rev. D* **107**, 015026 (2023), [arXiv:2109.07980 \[hep-ph\]](#).
- [42] G. Aad *et al.* (ATLAS), *Phys. Lett. B* **716**, 1 (2012), [arXiv:1207.7214 \[hep-ex\]](#).
- [43] S. Chatrchyan *et al.* (CMS), *Phys. Lett. B* **716**, 30 (2012), [arXiv:1207.7235 \[hep-ex\]](#).
- [44] F. del Aguila, M. Masip, and M. Perez-Victoria, *Nucl. Phys. B* **456**, 531 (1995), [arXiv:hep-ph/9507455](#).
- [45] P. H. Chankowski, S. Pokorski, and J. Wagner, *Eur. Phys. J. C* **47**, 187 (2006), [arXiv:hep-ph/0601097](#).
- [46] P. A. Zyla *et al.* (Particle Data Group), *PTEP* **2020**, 083C01 (2020).
- [47] T. Higaki, R. Kitano, and R. Sato, *JHEP* **07**, 044 (2014), [arXiv:1405.0013 \[hep-ph\]](#).
- [48] P. S. Bhupal Dev, R. N. Mohapatra, and Y. Zhang, *JHEP* **11**, 077 (2016), [arXiv:1608.06266 \[hep-ph\]](#).

- [49] M. Re Fiorentin, V. Niro, and N. Fornengo, *JHEP* **11**, 022 (2016), [arXiv:1606.04445 \[hep-ph\]](#).
- [50] P. Di Bari, P. O. Ludl, and S. Palomares-Ruiz, *JCAP* **11**, 044 (2016), [arXiv:1606.06238 \[hep-ph\]](#).
- [51] A. Atre, T. Han, S. Pascoli, and B. Zhang, *JHEP* **05**, 030 (2009), [arXiv:0901.3589 \[hep-ph\]](#).
- [52] K. Griest and D. Seckel, *Phys. Rev. D* **43**, 3191 (1991).
- [53] G. Bélanger, F. Boudjema, A. Goudelis, A. Pukhov, and B. Zaldivar, *Comput. Phys. Commun.* **231**, 173 (2018), [arXiv:1801.03509 \[hep-ph\]](#).
- [54] F. Staub, *Comput. Phys. Commun.* **185**, 1773 (2014), [arXiv:1309.7223 \[hep-ph\]](#).
- [55] W. Porod and F. Staub, *Comput. Phys. Commun.* **183**, 2458 (2012), [arXiv:1104.1573 \[hep-ph\]](#).
- [56] G. Belanger, F. Boudjema, A. Pukhov, and A. Semenov, *Nuovo Cim. C* **033N2**, 111 (2010), [arXiv:1005.4133 \[hep-ph\]](#).
- [57] P. Bechtle, O. Brein, S. Heinemeyer, G. Weiglein, and K. E. Williams, *Comput. Phys. Commun.* **181**, 138 (2010), [arXiv:0811.4169 \[hep-ph\]](#).
- [58] P. Bechtle, O. Brein, S. Heinemeyer, G. Weiglein, and K. E. Williams, *Comput. Phys. Commun.* **182**, 2605 (2011), [arXiv:1102.1898 \[hep-ph\]](#).
- [59] P. Bechtle, S. Heinemeyer, O. Stål, T. Stefaniak, and G. Weiglein, *Eur. Phys. J. C* **74**, 2711 (2014), [arXiv:1305.1933 \[hep-ph\]](#).
- [60] J. Aalbers *et al.* (DARWIN), *JCAP* **11**, 017 (2016), [arXiv:1606.07001 \[astro-ph.IM\]](#).
- [61] D. S. Akerib *et al.* (LZ), *Phys. Rev. D* **101**, 052002 (2020), [arXiv:1802.06039 \[astro-ph.IM\]](#).
- [62] E. Aprile *et al.* (XENON), *JCAP* **11**, 031 (2020), [arXiv:2007.08796 \[physics.ins-det\]](#).
- [63] M. L. Ahnen *et al.* (MAGIC, Fermi-LAT), *JCAP* **02**, 039 (2016), [arXiv:1601.06590 \[astro-ph.HE\]](#).
- [64] T. Daylan, D. P. Finkbeiner, D. Hooper, T. Linden, S. K. N. Portillo, N. L. Rodd, and T. R. Slatyer, *Phys. Dark Univ.* **12**, 1 (2016), [arXiv:1402.6703 \[astro-ph.HE\]](#).
- [65] R. K. Barman, G. Bélanger, B. Bhattacharjee, R. Godbole, D. Sengupta, and X. Tata, *Phys. Rev. D* **103**, 015029 (2021), [arXiv:2006.07854 \[hep-ph\]](#).
- [66] M. Blennow, E. Fernandez-Martinez, and B. Zaldivar, *JCAP* **01**, 003 (2014), [arXiv:1309.7348 \[hep-ph\]](#).
- [67] M. Aaboud *et al.* (ATLAS), *JHEP* **10**, 182 (2017), [arXiv:1707.02424 \[hep-ex\]](#).
- [68] A. M. Sirunyan *et al.* (CMS), *Phys. Rev. Lett.* **124**, 131802 (2020), [arXiv:1912.04776 \[hep-ex\]](#).
- [69] E. ACCOMANDO, D. Becciolini, A. Belyaev, S. De Curtis, D. Dominici, S. F. King, S. Moretti, and C. H. Shepherd-Themistocleous, *PoS DIS* **2013**, 125 (2013).
- [70] G. Aad *et al.* (ATLAS, CMS), *JHEP* **08**, 045 (2016), [arXiv:1606.02266 \[hep-ex\]](#).